Department of Signal Processing and Acoustics

Applications of Radiometric Measurements in Non-Contact Thermometry and Mesopic Photometry

Maksim Shpak

Aalto University

DOCTORAL DISSERTATIONS

Aalto University publication series
DOCTORAL DISSERTATIONS 167/2016
VTT SCIENCE 134

Applications of Radiometric Measurements in Non-Contact Thermometry and Mesopic Photometry

Maksim Shpak

A doctoral dissertation completed for the degree of Doctor of Science (Technology) to be defended, with the permission of the Aalto University School of Electrical Engineering, at a public examination held at the lecture hall S1 of the school on 16th September 2016 at 12.

Aalto University
School of Electrical Engineering
Department of Signal Processing and Acoustics
Metrology Research Institute

Supervising professor
Prof. Erkki Ikonen

Thesis advisor
Doc. Petri Kärhä

Preliminary examiners
Prof. Stephan Völker, Technische Universität Berlin, Germany
Assoc. Prof. Juha Toivonen, Tampere University of Technology, Finland

Opponents
Dr. Mohamed Sadli, Laboratoire commun de métrologie LNE-Cnam, France
Dr. Yoshi Ohno, National Institute of Standards and Technology, USA

Aalto University publication series
DOCTORAL DISSERTATIONS 167/2016

VTT SCIENCE 134

ISBN 978-952-60-6977-7 (printed)
ISBN 978-952-60-6978-4 (pdf)
ISSN-L 1799-4934
ISSN 1799-4934 (printed)
ISSN 1799-4942 (pdf)
http://urn.fi/URN:ISBN:978-952-60-6978-4

ISBN 978-951-38-8452-9 (printed)
ISBN 978-951-38-8453-6 (pdf)
ISSN-L 2242-119X
ISSN 2242-119X (printed)
ISSN 2242-1203 (pdf)
http://urn.fi/URN:ISBN:978-951-38-8453-6

Unigrafia Oy
Helsinki 2016

Finland

441 697
Printed matter

Author
Maksim Shpak

Name of the doctoral dissertation
Applications of Radiometric Measurements in Non-Contact Thermometry and Mesopic Photometry

Publisher School of Electrical Engineering

Unit Department of Signal Processing and Acoustics

Series Aalto University publication series DOCTORAL DISSERTATIONS 167/2016

Field of research Measurement Science and Technology

Manuscript submitted 4 March 2016 **Date of the defence** 16 September 2016

Permission to publish granted (date) 21 June 2016 **Language** English

☐ **Monograph** ☒ **Article dissertation (summary + original articles)**

Abstract

Radiometry deals with the measurement of electromagnetic radiation, its power and spectral and spatial distributions. Radiometric measurement techniques find use in many practical applications, including the measurement of visible light and its colour in photometry, measurement of temperature in pyrometry, chemical composition and physical properties in spectroscopy. The two main focus areas in this thesis are the non-contact measurement of temperature of a microscopic object and the practical application of mesopic photometry.

The subject in the study of the non-contact temperature measurement was a silicon microbridge emitter. The temperature of the microbridge was determined from its radiance spectrum in the visible and near-infrared regions. In contrast to previous studies, a grey body assumption was not used, and the determination of temperature was done by modelling spectral emissivity of the multi-layered structure of the microbridge. To accurately model the emissivity, the optical properties of the silicon at high temperatures were studied, which was not previously done for silicon with high doping concentrations. The extinction coefficient was determined from the radiance of a test sample placed in a furnace.

Mesopic photometry is a relatively new technique for measuring light, which takes into account the change of visual response in the overlapping region between the so-called day and night visions in the human eye. In this thesis, a novel dual channel photometer developed and characterised for the measurements in the mesopic luminance range is presented. The recommended system for mesopic photometry was published by the International Commission on Illumination (CIE) in 2010, and it provides mathematical tools for calculating mesopic quantities. The CIE mesopic system was studied in detail for this thesis and its applicability was analysed for all possible conditions in the mesopic range. Two problem areas were discovered at the edges of the mesopic range, where the mathematical model either did not converge or exhibited discontinuity. As a practical solution, a set of parameterised equations is presented that provides closed-form solutions and continuous transitions, with minimal deviation from the CIE system.

Keywords Radiometry, pyrometry, non-contact temperature, microbridge, microglow, silicon, extinction coefficient, photometry, mesopic, luminance

ISBN (printed) 978-952-60-6977-7 **ISBN (pdf)** 978-952-60-6978-4

ISSN-L 1799-4934 **ISSN (printed)** 1799-4934 **ISSN (pdf)** 1799-4942

Location of publisher Helsinki **Location of printing** Espoo **Year** 2016

Pages 91 **urn** http://urn.fi/URN:ISBN:978-952-60-6978-4

Tekijä
Maksim Shpak

Väitöskirjan nimi
Radiometristen menetelmien sovellukset lämpötilamittauksissa ja mesooppisessa fotometriassa

Julkaisija Sähkötekniikan korkeakoulu

Yksikkö Signaalinkäsittelyn ja akustiikan laitos

Sarja Aalto University publication series DOCTORAL DISSERTATIONS 167/2016

Tutkimusala Mittaustekniikka

Käsikirjoituksen pvm 04.03.2016 **Väitöspäivä** 16.09.2016

Julkaisuluvan myöntämispäivä 21.06.2016 **Kieli** Englanti

☐ **Monografia** ☒ **Yhdistelmäväitöskirja (yhteenveto-osa + erillisartikkelit)**

Tiivistelmä

Radiometria käsittelee sähkömagneettisen säteilyn mittaamista, sen tehoa ja spektrisiä ja spatiaalisia jakaumia. Radiometrisiä mittausmenetelmiä tarvitaan monessa käytännön sovelluksessa, mukaan lukien näkyvän valon ja värin mittaus fotometriassa, lämpötilan mittaus pyrometriassa, sekä kemiallisen koostumuksen ja fysikaalisten ominaisuuksien mittaus spektroskopiassa. Kaksi painopistealuetta tässä väitöskirjassa ovat mikroskooppisten kohteiden lämpötilan mittaus ilman kosketusta ja mesooppisen fotometrian käytännön toteutus.

Lämpötilan mittauksen kohteena oli piistä valmistettu mikrosilta-säteily-lähde. Mikrosillan lämpötila määritettiin sen radianssispektristä näkyvällä ja lähi-infrapuna-alueella. Toisin kuin aiemmissa tutkimuksissa, harmaan kappaleen oletusta ei ole tehty, vaan lämpötilan määritys tehtiin mikrosillan monikerrosrakenteen emissiivisyyttä mallintamalla. Tarkkaa mallinnusta varten tutkittiin piin optisia ominaisuuksia korkeissa lämpötiloissa, mitä ei ole aikaisemmin tehty raskaasti seostetulle piille. Piin ekstinktiokerroin määritettiin uunissa lämmitetyn piinäytteen radianssista.

Mesooppinen fotometria on suhteellisen uusi menetelmä valon mittaamiseen. Se ottaa huomioon ihmissilmän herkkyyden muutokset kirkkausalueella, jossa ns. yönäkeminen muuttuu päivänäkemiseksi. Tässä väitöskirjassa esitellään uusi kaksikanavainen fotometri, joka on kehitetty ja karakterisoitu mittauksiin mesooppisella luminanssialueella. Kansainvälinen valaistuskomissio (CIE) on julkaissut suosituksen mesooppiselle järjestelmälle vuonna 2010. Järjestelmä antaa matemaattiset työkalut mesooppisten suureiden laskemiseen. CIE:n mesooppista järjestelmää tutkittiin yksityiskohtaisesti tässä väitöskirjassa mukaan lukien sen soveltuvuus kaikille mahdollisille valaistusolosuhteille mesooppisella alueella. Kaksi ongelmakohtaa löydettiin mesooppisen alueen äärirajoilla, joissa matemaattinen malli ei konvergoinut tai oli epäjatkuva. Käytännön ratkaisuehdotuksena ongelmaan esitellään joukko parametrisoituja yhtälöitä, jotka takaavat jatkuvuuden yrittäen minimoida poikkeamat CIE:n järjestelmästä.

Avainsanat Radiometria, pyrometria, lämpötilan mittaus, mikrosilta, microglow, pii, ekstinktiokerroin, fotometria, mesooppinen, luminanssi

ISBN (painettu) 978-952-60-6977-7 **ISBN (pdf)** 978-952-60-6978-4

ISSN-L 1799-4934 **ISSN (painettu)** 1799-4934 **ISSN (pdf)** 1799-4942

Julkaisupaikka Helsinki **Painopaikka** Espoo **Vuosi** 2016

Sivumäärä 91 **urn** http://urn.fi/URN:ISBN:978-952-60-6978-4

Preface

The research work leading to this thesis was carried out during the years 2009–2016 at the Metrology Research Institute, Aalto University (Helsinki University of Technology before 2010) and at VTT MIKES Metrology (Centre for Metrology and Accreditation before 2015).

I am most grateful to my supervisor Prof. Erkki Ikonen for giving me the opportunity to work in the lab, to learn and contribute in the field of optical metrology, and for his expert guidance in the world of academia. I am also grateful to Doc. Petri Kärhä, for instructing my scientific work since before my master's thesis, for his insistence on maintaining the highest quality in research and publications, and for numerous on- and off-topic conversations.

I wish to thank Dr. Maija Ojanen-Saloranta for her guidance at the very beginning of my scientific career and for co-authoring several papers, and also Dr. Martti Heinonen for giving me the opportunity to do high temperature research at MIKES facilities. I also acknowledge my other co-authors and collaborators Prof. Sami Franssila, Dr. Lauri Sainiemi, Dr. Marek Šmíd and Dr. Geiland Porrovecchio.

A huge thank you goes to all my former colleagues at MRI for their otherwise uncredited support and collaboration, for creating excellent working atmosphere, and for many discussions on topics including electronics, music, cars, beer, science, but mostly the quality of coffee.

I thank the preliminary examiners Prof. Stephan Völker and Assoc. Prof. Juha Toivonen for their constructive feedback that helped improving the thesis.

The financial support provided by Tekniikan edistamissäätiö (TES) at the early stages of my post-graduate studies is greatly appreciated.

Finally, my family and friends have my warmest gratitude for their continuous support, patience and encouragements.

Espoo, August 2016,

Maksim Shpak

Contents

List of publications

This thesis consists of an overview and of the following publications which are referred to in the text by their Roman numerals:

I M. Shpak, P. Kärhä, M. Ojanen, E. Ikonen and M. Heinonen, "Optical temperature measurement method for glowing microcomponents," *International Journal of Thermophysics* **31**, 1762–1770 (2010).

II M. Shpak, L. Sainiemi, M. Ojanen, P. Kärhä, M. Heinonen, S. Franssila and E. Ikonen, "Optical temperature measurements of silicon microbridge emitters," *Applied Optics* **49**, 1489–1493 (2010).

III M. Shpak, P. Kärhä, G. Porrovecchio, M. Smid and E. Ikonen, "Luminance meter for photopic and scotopic measurements in the mesopic range," *Measurement Science and Technology* **25**, 095001, 7 pages (2014).

IV M. Shpak, P. Kärhä and E. Ikonen, "Mathematical limitations of the CIE mesopic photometry system," *Lighting Research and Technology,* 11 pages, published online before print, DOI:10.1177/1477153515599436 (2015).

Author's contribution

Publication I: The author developed the measurement set-up, performed the measurements and analysed the results.

Publication II: The author performed optical measurements and analysed the results. The author carried out the comparison of the optical non-contact results with results obtained from the contact temperature measurements.

Publication III: The author made the optical design of the instrument, characterisation measurements and uncertainty calculations.

Publication IV: The author made all mathematical analysis and parameterisation.

The author wrote first versions of all manuscripts and revised the texts on the basis of comments by co-authors and referees.

Symbols and abbreviations

List of abbreviations

CIE	International Commission on Illumination
MEMS	Micro-electromechanical systems
NMI	National metrology institute
S/P-ratio	Scotopic-photopic ratio
SI	International system of units
Si	Silicon
Si++	Boron-doped silicon
SiO_2	Silicon dioxide
SOI	Silicon-on-insulator

List of symbols

c	Speed of light in vacuum
h	Planck constant
I	Radiant intensity
I_{BB}	Radiant intensity of a black body
K_{cd}	Luminous efficacy of monochromatic radiation at λ_0
k	Boltzmann constant
k	Extinction coefficient
L_e	Radiance
L_{mes}	Mesopic luminance
L_p	Photopic luminance
L_s	Scotopic luminance
M	Normalisation factor
m	Adaptation ratio
n	Refractive index (real part)
$\bar{n}$	Complex refractive index

R_{SP}	Scotopic-photopic ratio
$\bar{r}$	Complex amplitude reflectance ratio
T	Absolute temperature
$\bar{t}$	Complex amplitude transmittance ratio
$V(\lambda)$	Photopic spectral luminous efficiency
$V'(\lambda)$	Scotopic spectral luminous efficiency
$V_{\mathrm{mes}}(\lambda)$	Mesopic spectral luminous efficiency
$\alpha_{\Omega,\lambda}$	Spectral directional absorptance
$\varepsilon_{\Omega,\lambda}$	Spectral directional emissivity
λ	Wavelength
λ_0	Wavelength at which the SI unit of candela is defined
$\rho_{\Omega,\lambda}$	Spectral directional reflectance
$\hat{\rho}_{\Omega,\lambda}$	Spectral directional hemispherical reflectance
$\tau_{\Omega,\lambda}$	Spectral directional transmittance
$\hat{\tau}_{\Omega,\lambda}$	Spectral directional hemispherical transmittance

1. Introduction

1.1 Background

The content of this thesis touches the fields of radiometry, pyrometry and photometry. While these fields are traditionally separated by their application, the underlying science and measurement techniques have much in common. In simple terms, they all measure electromagnetic radiation by optical means. In radiometry the concern is the determination of absolute power of radiation, pyrometry measures the temperature of an object by detecting the radiation emitted by it, and photometry is used to measure the visible part of electromagnetic spectrum in a way that correlates with the human vision.

Non-contact temperature measurement is typically associated with measuring the radiation in the infrared spectral range. Sir William Herschel discovered the heating effect of infrared radiation in 1800 by dispersing sunlight with a prism. Over the next 100 years, the works of Stefan, Boltzmann, Wien, Kirchhoff and Planck lead to precise definition of thermal radiation. Thermal radiation is not limited to an infrared region, but is comprising a wide spectrum of photon energies, generated by random kinetic movement of atoms in the matter at temperatures above absolute zero. This electromagnetic spectrum has a distribution that depends on the temperature of the emitting body, and it is described by the Planck's radiation law [1]. Pyrometry, or radiation thermometry, uses this relationship to determine temperature from measurements of spectral radiance.

Radiation thermometry has certain advantages over the contact temperature measurement methods. It can be used when the object is inaccessible due to being remote or contact-sensitive. For example, pyrometry is used to monitor temperature of semiconductor wafers during growth [2]. Another advantage is a very fast response, which allows measurement of rapidly changing phenomena [3], or measurement of fast moving ob-

jects [4]. At higher temperatures, radiation thermometry is the most accurate method for measurement of temperature. When realizing thermodynamic temperature scale at the level of national metrology institutes (NMI), the radiation thermometry is used to interpolate the temperature between silver and copper freezing points (1234.93–1357.77 K), and to extrapolate it above the copper freezing point [5–11]. Although pyrometry provides many benefits over the contact measurement, it is highly sensitive to the optical properties and the surface quality of the object being measured. Applying pyrometry to thin microscale structures introduces additional effects of optical interference, as the measured dimensions start to approach the wavelengths of the detected radiation.

Photometry is the field of science concerned with measuring light as it is perceived by a human eye. Its relation to the radiometry is through the spectral weighting functions that describe the sensitivity of the eye, as defined by the International Commission on Illumination (CIE) [12, 13]. Photometric measurements are normally performed with photometers, which are instruments that apply the spectral weighting, either by mathematically weighting the measured spectrum, or by filtering the light incident on the detector. The realization of the photometric quantities in many NMIs around the world is made with filtered detectors [14–18].

Because the goal in photometry is to obtain measurement results that correlate with the human vision, it has a necessary relation to physiology. Human eye uses cone cells for the day vision, rod cells for the night vision, and both types of cells simultaneously in dusk conditions. These vision regimes are called photopic, scotopic and mesopic, respectively. The growing importance of the mesopic vision in lighting design is related to the increased desire to optimise the use of energy [19]. The mesopic regime leads to many challenges in photometric measurements. Traditional single-channel instruments can only be used in combination with good knowledge about the spectral distribution of the light source. Without this knowledge, accurate measurements either require several instruments, or a new type of instrument designed specifically for mesopic measurements [20]. An additional challenge is the need to determine the state of the visual adaptation of the eye, which has a non-trivial dependence on the intensity and spectral quality of the incident light.

1.2 Thesis outline

Chapter 2 of this thesis presents the non-contact temperature measurement of microstructures. This includes measurement of optical parameters of doped silicon at high temperatures (publication I), modelling of spectral emissivity, and determination of the temperature of micro-emitters from their radiance spectra (publication II).

In chapter 3, the CIE mesopic photometry system is presented and mesopic measurement techniques are discussed. An instrument constructed for measurements in the mesopic range is presented (publication III). The CIE mesopic photometry system is also analysed from the mathematical point of view, identifying the areas of potential problems and suggesting solutions (publication IV). The thesis is summarised in chapter 4.

1.3 Scientific contribution

The thesis contains the following novel scientific results:

Publication I. Indirect measurement of optical properties of highly doped silicon at high temperatures was carried out by analysing the radiance spectrum emitted from a multi-layer structure of a silicon wafer. No data were available in literature for optical properties of doped silicon at high temperature at the time of publication. The authors are also not aware of any prior use of this method to determine the optical properties of a material.

Publication II. A method for non-contact measurement of temperature of a microscopic multi-layered structure was developed, and the measurement results were compared with contact temperature measurement. The method relies on fitting the modelled spectral emissivity to a measured radiance spectrum. The non-contact method was used to validate contact temperature measurement results and to provide connection between electrical properties and temperature. Prior attempts to optically measure temperature of micro-emitters did not take into account the effects of interference in the layers of the microstructure, which are now shown to be significant.

Publication III. A dual-channel instrument for simultaneous measurement of photopic and scotopic luminance was constructed. This is the first instrument that is capable of accurate measurements of luminance covering the whole mesopic range. The instrument is characterised in detail,

and paves a way for future development of practical mesopic instruments.

Publication IV. The extent of possible lighting conditions comprising the mesopic range is identified, and the CIE mesopic photometry system is analysed for all possible input values. Two problem areas are identified when the system is implemented according to CIE recommendation, related to sources with either very high or very low scotopic-photopic ratios. A set of closed-form equations is presented that parameterises the mesopic range. These results show the extent in which the CIE mesopic system can be practically applied and how to avoid problems with the CIE algorithm.

2. Temperature measurements on micrometre scale

2.1 Non-contact measurement of temperature

Traditional measurement of temperature involves conductive heat transfer between the measured object and the measurement instrument. To minimise the effect of thermal load, the thermal mass of the sensor in respect to the measured object is kept small. This becomes more challenging with the decreasing sizes of the object. In addition to the thermal load, making a physical contact with the object may inflict mechanical stress. Alternatively, the temperature can be determined by measuring the radiation emitted by the object, which does not require a physical contact.

All matter at non-zero temperature emits electromagnetic radiation. The spectral radiance of a perfect radiator, a so called black body, in a thermal equilibrium at a specific temperature is described by the Planck's law [1]

$$I(\lambda, T) = \frac{2hc^2}{\lambda^5} \frac{1}{\exp(\frac{hc}{\lambda kT}) - 1}, \tag{2.1}$$

where λ is the wavelength, h is the Planck constant, c is the speed of light, k is the Boltzmann constant and T is the temperature of the radiative surface. Figure 2.1 illustrates the change of intensity and the shift of peak wavelength of the black body radiation with the change of its temperature. Physical objects emit less energy than a black body, and the ratio between the two is emissivity

$$\varepsilon(\lambda, T) = \frac{I(\lambda, T)}{I_{BB}(\lambda, T)}, \tag{2.2}$$

where I refers to the spectral radiance of an actual object, and I_{BB} to the radiance of a black body at the same temperature. Emissivity is a property of the surface of the object, and usually varies with respect to the wavelength and temperature.

The non-contact measurement of temperature is typically a measurement of radiance, i.e. optical power emitted by a unit surface into a solid angle in certain direction. Determination of the temperature of real ob-

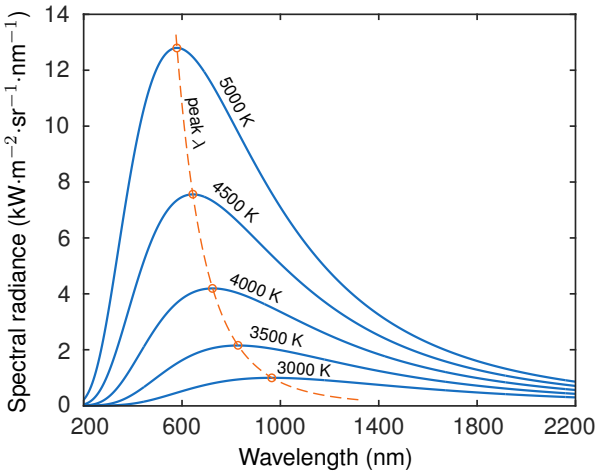

Figure 2.1. Black body radiation spectrum for several temperatures.

jects with equations 2.1 and 2.2 requires knowledge about the emissivity of the surface, and that poses one of the largest challenges in pyrometry. To minimize the uncertainty associated with emissivity, the radiation can be measured at two or more spectral bands, this is called multi-colour pyrometry [21, 22]. When variations of emissivity with wavelength in the spectral range of interest are very small, the surface is said to be behaving like a grey body. By making a grey body assumption, the temperature can be derived by applying multi-colour pyrometry, and by fitting the shape of the radiance spectrum to equation 2.1, even if the absolute value of emissivity is unknown.

For semi-transparent objects, knowledge of emissivity of the bulk material may not be sufficient, and the effective emissivity will depend on the geometry of the object. For microscale structures in particular, there is a possibility of interference due to inter-reflections from parallel surfaces, which may cause highly variable patterns in the spectral emissivity.

2.2 Microbridge-emitters

Microbridges are suspended miniature silicon structures, also known as microglows, micro-filaments, microheaters or thermal actuators [23]. A microbridge can be heated by passing an electrical current through it. Due to the low thermal mass and good heat conduction to the substrate through the anchor points, the temperature can be rapidly brought up

to the melting point of silicon and back down to the room temperature. At high temperatures, microbridges act as miniature incandescent light sources, and they have found use in some spectroscopic applications [24–27]. At elevated temperatures, the microbridge also tends to form an arc due to thermal expansion. This motion can be utilised as a cantilever for MEMS applications [28].

It is desirable to establish a relationship between the electrical power and the temperature of the microbridge. For this purpose a non-contact temperature measurement set-up was built, as presented in publication II. The measurement set-up consisted of a spectroradiometer coupled to a microscope objective, focused on the microbridge. The objective was collecting light from an area of approximately 25 µm in diameter, and the detected spectral range was 250–2500 nm. The measurement system was calibrated for spectral responsivity using a radiance source based on an integrating sphere [29]. An integrating sphere was used to uniformly fill the large light acceptance angle of the microscope objective.

The microbridges used in this study were approximately 400 µm long, 25 µm wide and 4 µm thick. An image of the microbridge is shown in figure 2.2. The microbridges were made of heavily boron-doped silicon (Si++), with a 200 nm thick silicon dioxide (SiO_2) layer coating on all surfaces. This creates a 3-layer cross-section with a Si++ layer sandwiched between two SiO_2 layers. Due to the high transmittance of SiO_2, and the semi-transparency of Si++ at certain wavelengths and temperatures, the structure produces high amount of oscillations in the emitted spectrum, caused by the interference in the layers. Determination of the temperature from this spectrum requires an accurate model for the effective spectral emissivity.

Other studies have been published, where the temperature of various similar micro-emitters was determined by optical means. Yuasa et al. [30] used a wideband detector for measurement of radiated power. In the works of Mastrangelo et al. [31] and Tu et al. [27] radiance was measured at several wavelength using bandpass filters. Fürjes et al. [32] used an array spectroradiometer to measure spectral radiance in the visible and the near-infrared range, and their results show oscillations in the measured spectrum, similar to our results. In all these studies, effects of interference on the emissivity of the filament were not considered, and temperatures were calculated using a grey-body assumption.

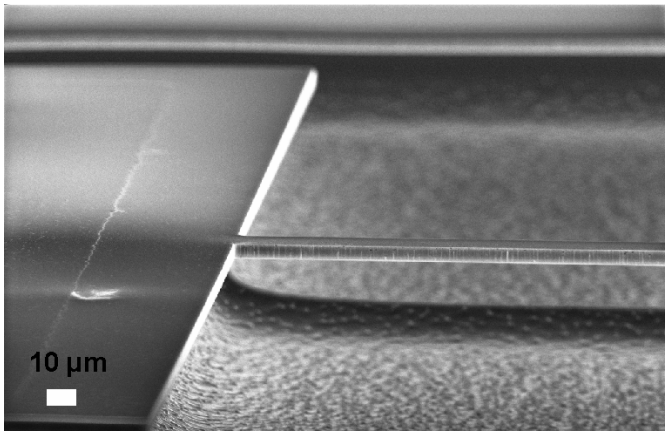

Figure 2.2. Scanning electron microscope image of a microbridge.

2.3 Optical properties of multi-layer structures

The emissivity of an object can be obtained directly by measuring its emitted spectrum when heated to a known temperature, and by comparing it to the calculated black body spectrum at the same temperature. Another method of obtaining the emissivity is through other optical properties of the material. For objects in thermal equilibrium, there is a relationship between absorptance, transmittance and reflectance due to the principle of conservation of energy. In the absence of any non-linear effects, this relationship is

$$\alpha_{\Omega,\lambda} + \hat{\tau}_{\Omega,\lambda} + \hat{\rho}_{\Omega,\lambda} = 1, \tag{2.3}$$

where $\alpha_{\Omega,\lambda}$ is the spectral directional absorptance, $\hat{\tau}_{\Omega,\lambda}$ is the spectral directional hemispherical transmittance and $\hat{\rho}_{\Omega,\lambda}$ is the spectral directional hemispherical reflectance of an object. The directional hemispherical quantities refer to a directional incidence and total hemispherical collection of light. In the case of objects with purely specular transmittance and reflectance, the spectral directional hemispherical quantities can be replaced by specular spectral directional quantities $\tau_{\Omega,\lambda}$ and $\rho_{\Omega,\lambda}$. According to the Kirchhoff's law, the thermal equilibrium can only be sustained if spectral directional absorptance is equal to emissivity, thus

$$\alpha_{\Omega,\lambda} = \varepsilon_{\Omega,\lambda}, \tag{2.4}$$

where $\varepsilon_{\Omega,\lambda}$ is the spectral directional emissivity.

Specular reflectance and transmittance at an interface between two media can be calculated using Fresnel equations [33, 34]. This requires complex refractive indices of both media, the angle of incidence, and the polar-

ization of incoming light. When dealing with the perpendicular angle of incidence only, the polarization state has no effect on the reflectance and transmittance. Simplified Fresnel equations for a single interface with perpendicular angle of incidence are

$$\bar{t}_{12} = \frac{2\bar{n}_1}{\bar{n}_1 + \bar{n}_2}, \tag{2.5}$$

and

$$\bar{r}_{12} = \frac{\bar{n}_1 - \bar{n}_2}{\bar{n}_1 + \bar{n}_2}, \tag{2.6}$$

where $\bar{n}_1$ and $\bar{n}_2$ are the complex refractive indices for the two media: $\bar{n} = n + ik$. Parameter n is the real part of the refractive index, and parameter k is the imaginary part, also known as the extinction coefficient. Values obtained from equations 2.5 and 2.6 are the complex amplitude transmission ($\bar{t}$) and reflection ($\bar{r}$) coefficients. To obtain intensity coefficients, the squares of absolute values are taken as

$$T = |\bar{t}|^2, \tag{2.7}$$

$$R = |\bar{r}|^2. \tag{2.8}$$

In multi-layered structures, inter-reflections occur between the layers, causing the amplitudes of the propagating waves to sum, as long as the thicknesses of the layers are smaller than the coherence length (temporal coherence) of the light [33]. Summing of amplitudes leads to constructive or destructive interference, depending on the phase difference of two wave fronts. The difference in phase is dependent on the difference in lengths of optical paths travelled by two interfering waves, which varies with wavelength. This leads to oscillations in spectral distribution of emitted radiation. For thicker layers no interference occurs, and intensities are summed instead of amplitudes. The total reflectance and transmittance of a stack of layered materials can be calculated using a transfer matrix method [33], or for simple systems, by calculating the sum of the geometric series of inter-reflections in the layers [35]. The thicknesses of the layers have a direct effect on interference, the change of thickness equal to just half of the wavelength means a 180° phase shift, thus it needs to be known accurately to successfully model the system.

The emissivity of a multi-layered object is calculated with equations 2.3 and 2.4 from the overall transmittance and reflectance of the object. In the case of objects where transmittance or reflectance are not purely specular, these values can not be calculated directly from the refractive indices, and the method requires measurements of the hemispherical quantities.

2.4 Emissivity and temperature of microbridge

Direct emissivity measurement of a microscopic structure at high temperatures is difficult, because accurate knowledge of the temperature of the object is needed. Therefore, the emissivity of the microbridge was modelled using the optical properties of materials. Because the microbridge is a layered structure, consisting of two SiO_2 layers with a Si++ layer in between, Fresnel equations were used to calculate the transmittance and the reflectance, and in turn the emissivity in accordance with equations 2.3 and 2.4. The real part of the refractive index of SiO_2 was taken from literature [36], and the extinction coefficient was estimated to be negligible. For the real part of the refractive index for doped silicon, a combination of data from several sources was used [37, 38], but for the extinction coefficient, no data extending to high temperatures and high doping concentration were found. The extinction coefficient depends on the absorptive properties of the material [37–40] which are directly influenced by the doping concentration. Absorption is also heavily dependent on temperature [37–39], which would make the extrapolation of the existing data unreliable.

To determine the extinction coefficient of Si++, a piece of silicon-on-insulator (SOI) wafer was placed in a furnace, and its radiance was measured with a spectroradiometer focused on its surface. A SOI wafer consisted of a thick silicon substrate, a thin buried oxide layer (SiO_2), a silicon device layer with high level of doping (Si++) and a thermally grown top oxide layer (SiO_2). The heating provided by the furnace was uniform, and the temperature of the wafer was measured with a thermocouple. The emissivity was determined from the measured spectral radiance and temperature with Planck's equation 2.1. The measurement set-up and the analysis method are presented in publication I. The structure of SOI is similar to that of a microbridge, the cross-sections of both are shown in figure 2.3. The level of the boron-doping in the middle silicon layer was the same as in the studied microbridge, and equalled approximately 5×10^{18} cm^{-3}. The substrate layer was un-doped silicon. By modelling the emissivity of the SOI wafer, the missing optical parameters were determined by fitting the model to the emissivity obtained from measurements. In addition to the extinction coefficient of Si++, the thicknesses of the layers had to be fitted.

The diffuse reflectance component of the SOI-wafer was measured to

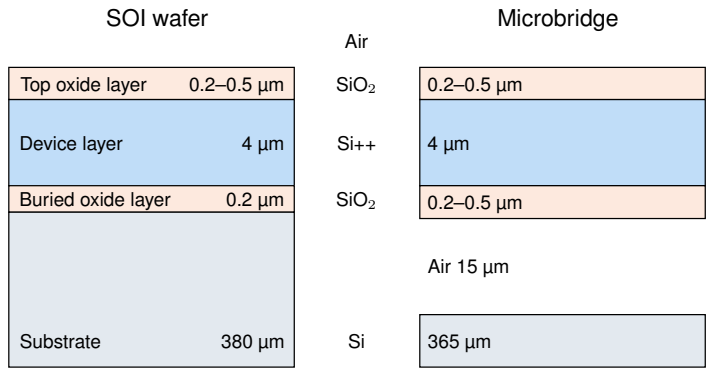

Figure 2.3. Cross-sections of the studied SOI wafer and the microbridge. The original thicknesses of the SiO_2 layers were 200 nm, but when operated at elevated temperatures, the thicknesses of the layers exposed to air may have increased.

be about 0.02 % at room temperature and at the wavelength of 633 nm. This was considered indicative of a smooth surface quality, and the diffuse components were not taken into account in further calculations. As the microbridge itself was manufactured from the same SOI-wafer, the same surface quality assumptions were applicable.

Measurements were performed in the 400–2500 nm spectral range and at the temperatures of 719 °C, 914 °C and 1109 °C. Figure 2.4 shows the spectral emissivity calculated from the measurement of radiance of a SOI-wafer at a temperature of 1109 °C, as well as the fitted emissivity model.

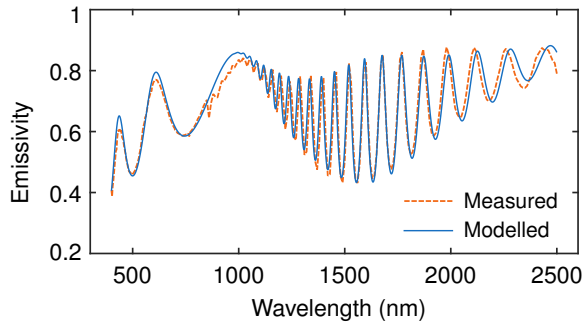

Figure 2.4. Spectral emissivity measured for a SOI wafer at 1109 °C.

It was determined experimentally from the emissivity model, that the fast oscillation in the near-infrared spectrum are mainly governed by the parameters of the Si++ layer, its thickness and complex refractive index. The amplitude of these oscillations is related to the extinction coefficient in this layer. Slower oscillations in the spectrum are caused by inter-

reflections in the top SiO_2 layer. The extinction coefficients of Si++ is obtained by fitting the parameters of emissivity models, and are shown in figure 2.5 for the 3 temperatures used. The obtained values of extinction coefficient are generally higher than those found in literature for lower temperatures and lower doping concentrations [37, 39, 41–43].

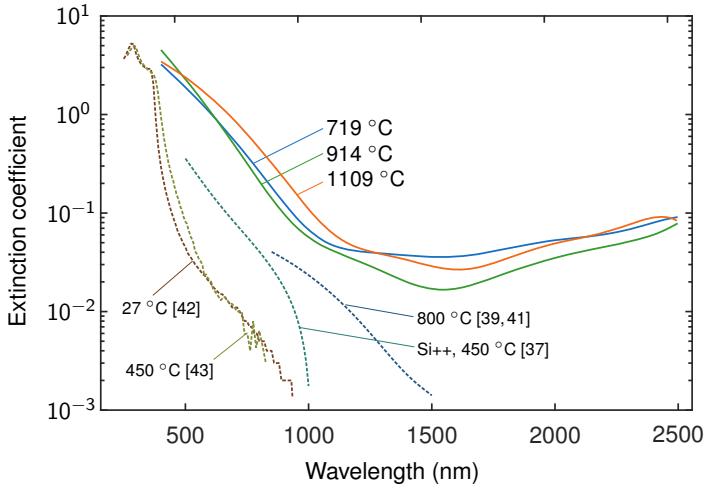

Figure 2.5. Obtained spectral extinction coefficient of highly doped silicon for 3 temperatures (solid lines), and comparison data from literature (dashed lines).

The measurement of the temperature of the microbridge was then performed using the emissivity model with the determined optical parameters. This was achieved by fitting the measured radiance spectrum to the product of modelled emissivity spectrum and the black body radiation spectrum, by varying the temperature parameter. However, the thicknesses of the layers in the microbridge were known only approximately, and remained as fitted parameters alongside the temperature. Figure 2.6 presents the radiance spectrum measured for the microbridge, with the best obtainable fit of the radiance model. The temperature obtained for this graph was 940 °C. These results are presented in more detail in publication II.

2.5 Comparison of pyrometry and contact thermometry

Non-contact temperature measurements were compared with contact measurements in publication II. In both cases, the temperature was measured as a function of the heating power. Also the electrical resistance of the operating microbridge was determined from the applied voltage and the

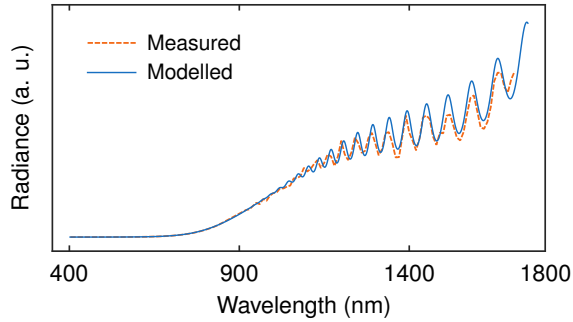

Figure 2.6. Normalised radiance spectra of the microbridge at 940 °C, measured curve shown with dashed line, modelled curve with solid line.

current readings.

Comparing normalised resistance values as a function of heating power for optical and contact measurements, there appeared to be an offset of approximately 22 mW, as shown in figure 2.7a. The overall resistance reading includes the resistance caused by the probe contacts and the resistance of the microbridge itself. The change of resistance in the microbridge with temperature can be explained by the change of resistivity of the semiconductor layer, and by the change of geometry of the microbridge due to a thermal expansion. The peak resistance should therefore always occur at the same temperature for a given microbridge. The apparent offset in supplied power of the contact measurement can be due to the heat loss through the thermocouple, due to the electrical losses in the probe contacts or due to the variations in the microbridge samples.

The results for temperature reading as a function of heating power are shown in figure 2.7b. The rate of change is very similar between the two curves up to 1000 °C, but there is an offset in either the temperature or the power values. Contact temperature data shifted by the 22 mW, that was obtained by comparing normalised peak resistances, is shown with the dashed line, and it has a very good agreement with the optical measurement data.

For temperatures below 600 °C, the optical method is likely less accurate due to low signal levels, and at temperatures above 1000 °C, the contact method is likely underestimating the temperature readings due to the increased thermal losses in the contact heat transfer.

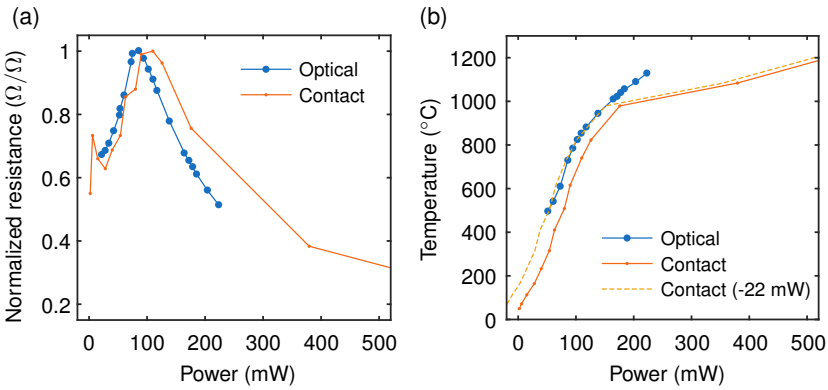

Figure 2.7. Comparison of the non-contact and contact temperature measurements. (a) Normalised resistance as a function of input power. (b) Temperature as a function of input power, including a contact measurement data offset by 22 mW (dashed line).

3. Mesopic photometry

3.1 Human vision system and photometry

A human eye is a complicated instrument, particularly in the way it adapts to different lighting conditions, changing its spectral and spatial sensitivity. The two extreme ends of adaptation are the so-called day vision, where only cone cells are active, and the night vision, where only the rod cells are active. These are referred to as photopic and scotopic vision regimes, respectively. The intermediate region, where both types of cells are active simultaneously is called the mesopic region [12]. Figure 3.1 shows lighting conditions under which the three types of vision are prevalent, as well as approximate luminance levels.

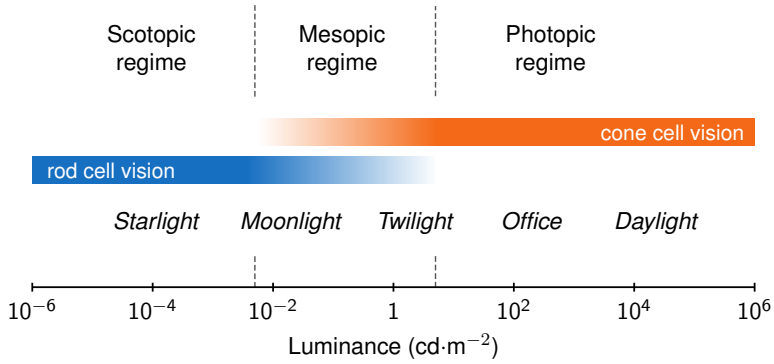

Figure 3.1. Lighting conditions and vision regimes.

There are 3 types of cone cells with differing spectral sensitivities, which gives the eye its ability to perceive colour in the photopic vision regime. The highest concentration of the cone cells is in the central part of the retina, called a fovea. The rod cells are more sensitive to light, but do not distinguish colour. Also, the rod cells are mostly found outside the fovea, meaning that most of the scotopic vision comes from the periphery.

The adaptation of the eye depends on the level of signal on both types of

photoreceptors. At low light levels, the high sensitivity of rod cells dominates the response. As the rod cells saturate, the high light levels are detected only by the cone cells. Due to the differences in spectral sensitivities, the adaptation depends on the spectral quality of the incident light. It has also been shown that adaptation happens at different rates when light levels are increasing or decreasing, and that adaptation happens both locally and globally on the surface of the retina [44].

The CIE is an international authority and standardisation body on photometry, and it provides guidelines for performing photometric measurements. Although the performance of the human visual system varies between individuals, a harmonised system of performing measurements is necessary. To address this, CIE defines a "Standard Observer", which performs in a way that correlates with average human vision. For the day and night vision regimes, CIE defines photopic and scotopic spectral luminous efficiency functions [12]. These functions are often denoted by $V(\lambda)$ and $V'(\lambda)$, respectively. Until recently, there has been no agreed definition for a mesopic luminous efficiency function or for the level of adaptation.

3.2 CIE mesopic photometry system

For the mesopic region there is no single spectral luminous efficiency function. The spectral responsivity is dependent on the state of adaptation. Several studies have been conducted in attempt to provide a continuous bridge between the scotopic and the photopic regions, using either the apparent brightness or the visual performance as the adaptation criterion [45–47]. As the physiological process of visual adaptation is extremely complex [48], it is necessary to have a certain degree of simplification. CIE has recently published a recommendation on a performance-based system of mesopic photometry (CIE191) [49]. According to this recommendation, the mesopic luminous efficiency function is a linear combination of the photopic and the scotopic luminous efficiency functions

$$V_{\mathrm{mes}}(\lambda) = \frac{1}{M(m)}[mV(\lambda) + (1-m)V'(\lambda)], \tag{3.1}$$

where m is the adaptation ratio, and M is a normalisation factor, which ensures that the peak value of $V_{\mathrm{mes}}(\lambda)$ is 1. When $m = 0$, the vision is purely scotopic, and $V_{\mathrm{mes}}(\lambda) = V'(\lambda)$. When $m = 1$, the vision is purely photopic, and $V_{\mathrm{mes}}(\lambda) = V(\lambda)$. Figure 3.2 shows the dependence of the luminous efficiency function on the adaptation ratio.

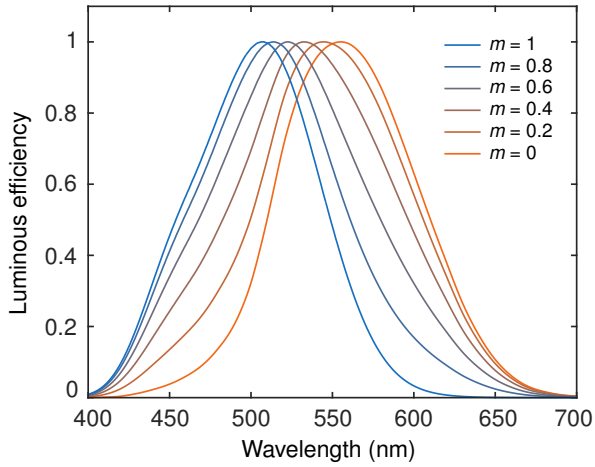

Figure 3.2. Mesopic luminous efficiency functions for various adaptation levels.

To calculate photometric quantities, the measured spectral power distribution is integrated with the luminous efficiency weighting, and scaled by the luminous efficacy at the wavelength of the peak sensitivity. For the case of mesopic luminance

$$L_{\mathrm{mes}} = \frac{K_{\mathrm{cd}}}{V_{\mathrm{mes}}(\lambda_0)} \int V_{\mathrm{mes}}(\lambda) L_{\mathrm{e}}(\lambda) \mathrm{d}\lambda, \tag{3.2}$$

where $L_{\mathrm{e}}(\lambda)$ is the spectral radiance, $\lambda_0 \approx 555.016$ nm is the wavelength in standard air at which the SI unit of candela is defined [12], and $K_{\mathrm{cd}} = 683$ lm/W is the luminous efficacy of monochromatic radiation at λ_0 [50]. Alternatively, mesopic luminance can be expressed as a function of the photopic and scotopic luminances L_{p} and L_{s} as

$$L_{\mathrm{mes}} = \frac{m L_{\mathrm{p}} + (1-m) L_{\mathrm{s}} V'(\lambda_0)}{m + (1-m) V'(\lambda_0)}, \tag{3.3}$$

where $V'(\lambda_0)$ is the value of the scotopic luminous efficiency function at λ_0 [13]. Detailed derivation of the equation 3.3 is shown in the appendix of publication IV.

There is a characteristic ratio between the scotopic and the photopic quantities measured for a given light source, called the S/P-ratio, or R_{sp}. Knowing the S/P-ratio allows calculation of the mesopic quantity from either the scotopic or the photopic quantity. It should be noted that for a typical luminance measurement, the measured light is reflected from a surface, which will alter the spectral distribution and hence the S/P-ratio, increasing the uncertainty of measurement that relies on just photopic or scotopic measurement to calculate mesopic value.

Adaptation ratio m depends on lighting conditions of the surrounding scene. For a static condition, where the scene is uniform, and the eye is fully adapted, CIE191 gives a formula for the relation between the adaptation level m and the mesopic luminance L_{mes} of the scene as

$$m = a + b \log_{10}(L_{\mathrm{mes}}/L_0), \quad \text{for} \quad 0 \leq m \leq 1, \tag{3.4}$$

where $L_0 = 1$ cd·m^{-2}, and the values for parameters a and b are approximately $a = 0.7670$ and $b = 0.3334$. It also sets limits for the mesopic range, stating that for the values of the mesopic luminance $L_{\mathrm{mes}} \geq 5.0$ cd·m^{-2}, the adaptation level is $m = 1$ and the vision is purely photopic. For the values of $L_{\mathrm{mes}} \leq 0.005$ cd·m^{-2}, the adaptation level is $m = 0$ and the vision is purely scotopic. Since equations 3.3 and 3.4 are functions of each other, the proposed solution algorithm is an iterative calculation of these two functions with a starting value of $m = 0.5$, which is repeated until a convergence is achieved.

In practice, the luminance distribution of the scene is usually not uniform, and the state of adaptation is determined by luminance in a certain field of view, with a specific weighting. This is referred to as an adaptation field. At the moment of writing, the work on definition of the adaptation field is still ongoing in the technical committees of the CIE.

3.3 Instruments for mesopic measurements

The measurements of photometric quantities are analogous to radiometric measurements, with the addition of spectral weighting that matches one of the luminous efficiency functions. This weighting can be applied in the form of a band pass filter, or as numerical integration of a spectral measurement.

The area in which mesopic photometry has the most potential impact is street lighting optimisation. Instruments commonly used in this application are luminance meters. These instruments typically employ focusing optics and a filtering element to match the spectral responsivity to the luminous efficiency function. The detection is done either with a single element detector and a defined field of view, or with a matrix detector, such that the distribution of the whole scene can be imaged at once. Spectral instruments can be used as well, although the need to disperse the light means they are usually slower and can not image a whole scene at once.

For the measurement of mesopic luminance, a single-channel instru-

ment is generally not enough. The dependence of the mesopic spectral luminous efficiency on the level of adaptation means that at least two spectrally separated channels are needed to estimate the mesopic luminance. Only in the case where the spectral composition of measured light is known, the mesopic luminance can be calculated from a single channel measurement by performing a spectral mismatch correction, analogously to the spectral mismatch correction used in the realisation of the candela with $V(\lambda)$-filtered photometers [18]. In the street lighting applications, normally all measured light is reflected from surfaces that significantly alter the spectrum, for example the reflectance of asphalt can distort the spectral shape of source light by up to 20 % [51]. This has a large effect on the uncertainty of spectral mismatch correction. The error depending on the light source can be between 5–10 %, which reduces to under 1 % with the use of two detection channels, as shown in publication III.

For simultaneous measurement of photopic and scotopic luminance in the mesopic range, a novel, dual-channel spot luminance meter was constructed. The incoming light is separated in the instrument into two detection channels with a beamsplitter. One channel has an optical filter matching the photopic spectral responsivity, and the other channel has a filter matching the scotopic spectral responsivity. Signals from the silicon photodetectors are measured with a switched-integration amplifier [52]. The detection part of the instrument is shown in figure 3.3. By combining the signals from the two channels, a mesopic luminance of any adaptation level can be obtained, as is evident from equation 3.3. The instrument is capable of fast measurements in the whole mesopic range: $0.005\ \mathrm{cd{\cdot}m^{-2}} \leq L_{\mathrm{mes}} \leq 5\ \mathrm{cd{\cdot}m^{-2}}$. At the lowest end of the range, a 0.5 % standard deviation of mean of the measured signal is attainable with < 1 second of integration time.

The instrument was thoroughly characterised for absolute spectral responsivities of both channels, linearity, stray light sensitivity and polarization dependence; also the effect of temperature variations was estimated. The expanded measurement uncertainty at the lowest end of the mesopic range is 2.2 % with 95 % level of confidence, traceable to the luminance and spectral radiance scales of the Metrology Research Institute [18, 29].

The uncertainty budget of the photopic-scotopic luminance meter is presented in detail in publication III. We also suggest that the dual-channel filtered instrument is the optimal way of implementing a reliable mesopic

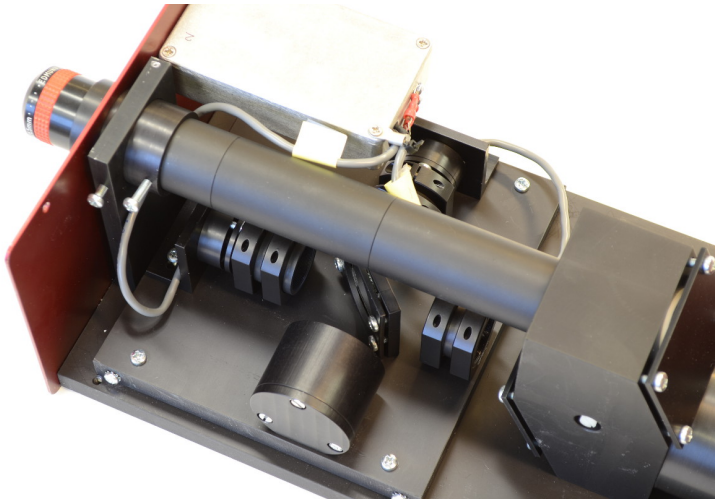

Figure 3.3. Detection part of the photopic-scotopic dual channel luminance meter (covers removed).

luminance measurement. This prototype luminance meter serves as a study platform for the design of future mesopic instruments, identifying the issues specific to the filtered, dual-channel design. One of these issues is sensitivity to polarization due to the need to use a beamsplitter, the other is temperature sensitivity of absorptive optical filters. Future instruments will also need to employ the measurement of adaptation level, which also requires a dual-channel or a spectral measurement.

At the moment, there is no agreed definition of the adaptation field. Because the adaptation level m depends on the luminance in the adaptation field, it is not possible to perform independent measurements of mesopic luminance without making assumptions about the adaptation ratio.

3.4 Mathematical analysis of CIE mesopic photometry system

According to the CIE 191 mesopic system [49], adaptation level m depends on the mesopic luminance L_{mes} in the adaptation field, as shown in equation 3.4. The mesopic luminance itself is calculated using the adaptation level m and the photopic and scotopic luminances L_{p} and L_{s}, as shown in equation 3.3. To solve this pair of interdependent equations, CIE 191 presents an iterative algorithm, where m_0 is given an initial value of 0.5, and it is used to calculate $L_{\mathrm{mes},1}$, after which a new value m_1 is calculated, and so on. This process is repeated until the value m_n converges to an unambiguous value of m.

The mesopic luminance L_{mes} is obtained from the photopic and scotopic luminances L_{p} and L_{s} with equations 3.3 and 3.4. It can thus be presented as a 3D graph $L_{\mathrm{mes}}(L_{\mathrm{p}}, L_{\mathrm{s}})$. Because of the monotonic relationship between L_{mes} and m, the adaptation level can also be presented in 3D graph as $m(L_{\mathrm{p}}, L_{\mathrm{s}})$. The ratio of the scotopic luminance to the photopic luminance measured from the same scene is the S/P-ratio, or R_{sp}, and so the mesopic luminance and the adaptation field can also be shown as functions of the photopic luminance and the S/P-ratio as $L_{\mathrm{mes}}(L_{\mathrm{p}}, R_{\mathrm{sp}})$ and $m(L_{\mathrm{p}}, R_{\mathrm{sp}})$. These relationships give a convenient way of visualising and analysing the entire mesopic range.

By examining equations 3.3 and 3.4 that lead to the function $m(L_p, L_s)$, it is evident that the limits set by $0 < m < 1$ restrict the set of input parameters that produce adaptation levels within the mesopic range. At the high end, where $L_{\mathrm{p}} \geq 5$ cd·m^{-2}, m can only achieve the value of 1. But at the low end, both L_{p} and L_{s} can individually be arbitrarily small or even zero, and can still lead to $m > 0$, making the input parameter space infinitely large. However, the range of possible values of R_{sp} is limited to approximately 0.01–73, as shown in publication IV, which in turn limits the practically achievable mesopic space as presented in figure 3.4. Using the S/P-ratio as the second input parameter reshapes the allowed input parameter space into a rectangle, which is useful in subsequent analyses.

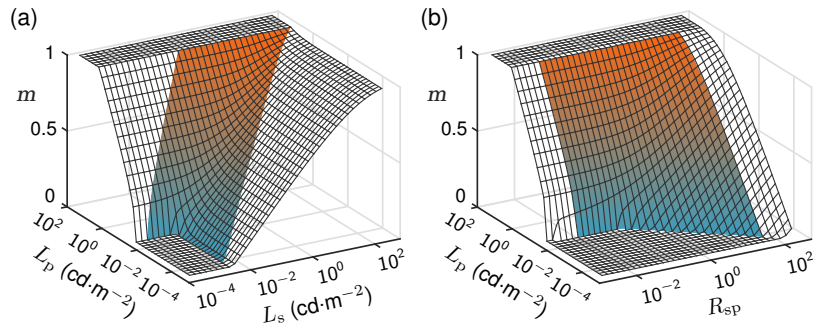

Figure 3.4. (a) Adaptation level as a function of photopic and scotopic luminance and (b) as photopic luminance and S/P-ratio. Shaded area shows all possible mesopic values.

Having defined the limits of the allowed input values, we analysed the iterative algorithm for all possible conditions, and identified the main problem areas. For very high S/P-ratios, the iterative algorithm may be unable to converge to a single solution. This can happen only for S/P-ratios over 17, as shown in figure 3.5. The solution can nevertheless be found by other means, for example by solving the pair of equations 3.3 and

3.4 numerically. A vast majority of light sources, however, do not approach such high S/P-ratios, which is only possible with fairly narrowband, short wavelength sources. For example, a cool white LED has $R_{\mathrm{sp}} \approx 2.3$, and a deep blue (450 nm) LED has $R_{\mathrm{sp}} \approx 28$. The extreme values of S/P-ratio can potentially be found in some unintended lighting conditions, such as light from indication lamps, advertisement boards or the light from cinema screens.

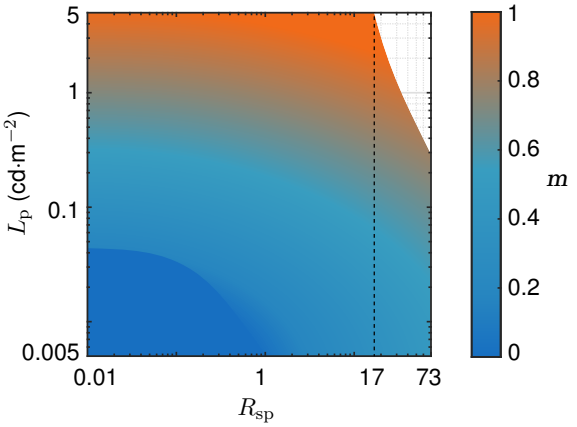

Figure 3.5. Adaptation level m as a function of L_{p} and R_{sp}. In the non-shaded area the iterative model does not converge.

Another, considerably more difficult issue is the discontinuity at the low edge of the mesopic range. The discontinuity exists at $R_{\mathrm{sp}} < 1$, when transitioning from the scotopic into the mesopic range. This transition is illustrated in figure 3.6 as mesopic luminance as a function of photopic luminance for several S/P-ratio values, in both linear and logarithmic scales. The main cause of the discontinuity is the lower limit set by the definition to the mesopic luminance, where the adaptation level is forced to be zero for all values of $L_{\mathrm{mes}} \leq 0.005$ cd·m^{-2}, meaning that $L_{\mathrm{mes}} = L_{\mathrm{s}} = L_{\mathrm{p}} R_{\mathrm{sp}}$. This leads to situations, where on the high side of discontinuity $m > 0$ and $L_{\mathrm{mes}} > 0.005$ cd·m^{-2}, but on the low side of discontinuity $m = 0$, and $L_{\mathrm{mes}} < 0.005$ cd·m^{-2}. The discontinuity gap becomes larger with smaller S/P-ratios. This issue is not caused by the solution algorithm, but it is instead a direct consequence of the definition of the mesopic luminance.

In an effort to obtain a continuous and closed-form solution for the mesopic range, a set of formulae was constructed for $m(L_{\mathrm{p}}, R_{\mathrm{sp}})$, that approximate the CIE mesopic model. To avoid discontinuities, the requirement for the adaptation level to be zero for all values of $L_{\mathrm{mes}} < 0.005$ cd·m^{-2} had to be dropped. The new requirements are such that $m = 0$, when both

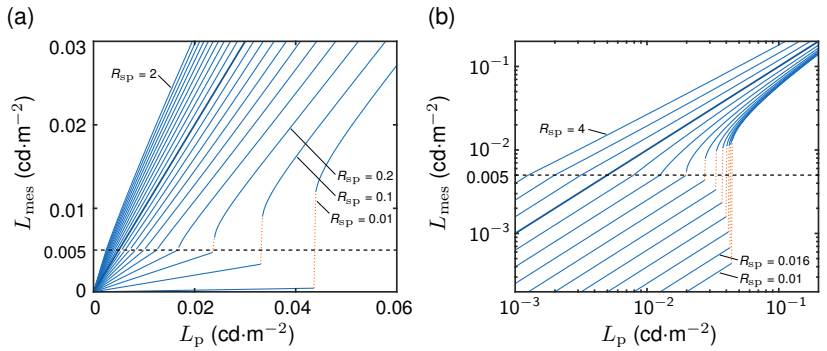

Figure 3.6. Discontinuity at the low end of the mesopic range, shown as $L_{mes}(L_p)$ for several values of R_{sp}. (a) Shown in linear scales, for $0.1 \leq R_{sp} \leq 2$ with a step of 0.1, and also for $R_{sp} = 0.01$. (b) Shown in logarithmic scales for 14 logarithmically distributed values of $0.01 \leq R_{sp} \leq 4$. Bold line on both graphs indicates $R_{sp} = 1$, and dotted lines connect discontinuous points.

$L_p < 0.005$ cd·m^{-2} and $L_s < 0.005$ cd·m^{-2}. The whole luminance range is divided here into 4 possible conditions, where $L_1 = 0.005$ cd·m^{-2} and $L_2 = 5$ cd·m^{-2}:

1. When $L_p \leq L_1$ and $R_{sp} \leq 1$, the value of m is always 0.
2. When $L_p \geq L_2$, the value of m is always 1.
3. When $L_1 < L_p < L_2$ and $R_{sp} \leq 1$, the value of m is given by an explicit equation in publication IV, involving L_p and R_{sp}.
4. When $L_p < L_2$ and $R_{sp} > 1$, the value of m is given by another explicit equation in publication IV, involving L_p and R_{sp}.

The intent was to make the parameterisation with minimal deviations from the CIE mesopic model, but for condition 3, there is an unavoidable deviation due to the discontinuity in the CIE mesopic model, as shown in figure 3.7. Outside the problem areas, the difference in m between the CIE model and parameterisation is below 0.005. Its effect on the mesopic luminance value L_{mes} is then below 0.5 %. For very high S/P-ratios ($R_{sp} > 40$), the difference in m is below 0.013, and its effect on L_{mes} is under 10 %.

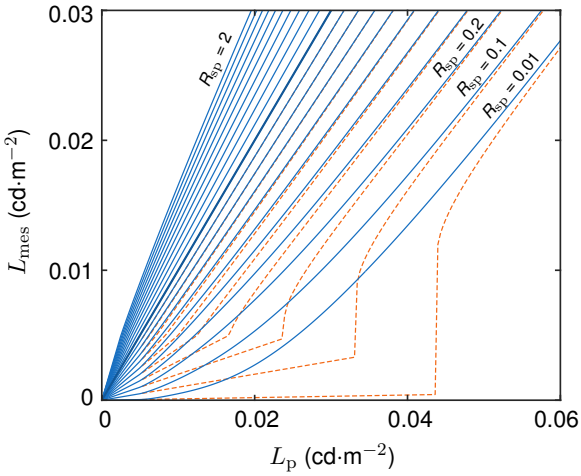

Figure 3.7. Parameterised function $L_{\mathrm{mes}}(L_{\mathrm{p}})$ for several values of R_{sp} (solid lines), and values calculated using CIE iterative algorithm (dashed lines).

4. Summary

In this thesis, a method for temperature measurement of a microscopic multi-layered structure was developed. The structure studied was a micro-emitter fabricated in silicon. The temperature measurement method consists of fitting Planck's equation to the measured relative spectral radiance, by adjusting the parameters of the modelled emissivity. The relative spectral radiance was measured by capturing the light with a microscope objective and guiding it into a spectroradiometer. The measurement system was calibrated for the spectral responsivity with a source based on an integrating sphere. The model for the emissivity is based on dimensions of the layers in the structure and the optical properties of the materials. To obtain the optical properties needed, an indirect measurement method was employed, where the extinction coefficient of highly doped silicon was determined from the radiance of a layered structure at a known temperature. The temperature obtained with the non-contact method was compared with a contact measurement, and the comparison showed good agreement at temperatures up to 1000 °C, with an apparent offset in the input power of approximately 22 mW in the 0–200 mW range, which is equivalent to approximately 100 °C difference in temperature. This difference can be explained by electrical losses in the power supply probes or by the loss of heat through the thermocouple probe. There can also be variations in the resistance of different microbridge samples that would manifest in the similar way. At temperatures above 1000 °C, the contact method gives significantly lower readings, which is likely due to increased thermal losses via the thermocouple.

The field of mesopic photometry has seen major developments in the recent years. Most importantly the CIE has published a recommended system for mesopic photometry. In this thesis, one of the first studies in implementing the mesopic photometry was carried out. A novel type of dual-channel instrument was constructed and characterised. The instrument is able to measure photopic and scotopic luminances simultaneously. The instrument provides a study platform for future realisations of

mesopic photometry. It shows the benefits of the dual-channel configuration as well as potential problem areas. At the moment of writing, there is no published definition for the adaptation field, which prevents from performing true, independent mesopic measurements without assumptions about the level of adaptation. The work is undergoing in CIE to produce a recommendation for the adaptation field in the near future. The outcome of CIE's recommendation will affect the type of instruments that will be practical for mesopic measurements. If the adaptation field will be fixed to a specific shape, a fixed field-of-view instrument, like the one presented here, will be sufficient to perform the measurements. It will also have certain advantages over a camera-based instrument, such as typically higher sensitivity, higher accuracy and lower cost. If the adaptation field will instead have a dynamic, task-dependent shape, a camera-based instrument will be necessary, but it will nevertheless benefit from a dual-channel configuration that is presented here.

With the publication of the new system for mesopic photometry, CIE has provided tools to perform measurements that better approximate the human vision under low lighting conditions. The new system employs an iterative calculation method to obtain the level of adaptation, which is the measure defining the mesopic spectral sensitivity for a particular condition. Due to the nature of the iterative method, the relationship between the luminance of the adaptation field and the level of adaptation is non-trivial, and can not be solved analytically. In this thesis, the CIE mesopic system was analysed mathematically. The mesopic conditions were identified, and the adaptation level was calculated for all possible values. Two problem areas were identified, in one of which the iterative method does not converge, and the other where the mesopic luminance exhibits discontinuity. The first problem can be addressed without redefining the mesopic system, while the second problem is shown to be caused by the definition itself. A set of closed-form equations were constructed that closely approximate the CIE mesopic system. These equations allow calculating the adaptation level without the use of the iterative algorithm. Also, the discontinuity region is smoothed out to provide a continuous mesopic luminance.

References

[1] M. Planck. Über das Gesetz der Energieverteilung im Normalspectrum. *Annalen der Physik*, 309(3):553–563, 1901.

[2] G. Feng, K. Oe, and M. Yoshimoto. Temperature dependence of Bi behavior in MBE growth of InGaAs/InP. *Journal of Crystal Growth*, 301-302:121–124, 2007.

[3] G. A. Lyzenga and T. J. Ahrens. Multiwavelength optical pyrometer for shock compression experiments. *Review of Scientific Instruments*, 50(11):1421, 1979.

[4] M. De Lucia and G. Masotti. A Scanning Radiation Thermometry Technique for Determining Temperature Distribution in Gas Turbines. *Journal of Engineering for Gas Turbines and Power*, 117(2):341, 1995.

[5] H. Preston-Thomas. The International Temperature Scale of 1990 (ITS-90). *Metrologia*, 27(1):3–10, 1990.

[6] N. J. Harrison, N. P. Fox, P. Sperfeld, J. Metzdorf, B. B. Khlevnoy, R. I. Stolyarevskaya, V. B. Khromchenko, S. N. Mekhontsev, V. I. Shapoval, M. F. Zelener, and V. I. Sapritsky. International comparison of radiation-temperature measurements with filtered detectors over the temperature range 1380 K to 3100 K. *Metrologia*, 35(4):283–288, 1998.

[7] F. Sakuma, L. Ma, and J. Hartmann. Intercomparison of radiation temperature scales between PTB and NMIJ from 1100 °C to 2500 °C. In *SICE 2002. Proceedings of the 41st SICE Annual Conference*, volume 5, pages 58–62, 2002.

[8] J. Fischer, M. Battuello, M. Sadli, M. Ballico, S. N. Park, P. Saunders, Y. Zundong, B. C. Johnson, E. van der Ham, F. Sakuma, G. Machin, N. Fox, W. Li, S. Ugur, and M. Matveyev. Uncertainty Budgets for Realization of ITS-90 by Radiation Thermometry. In *Temperature: Its Measurement and Control in Science and Industry, AIP Conf. Proc.*, volume 684, pages 631–638. AIP, 2003.

[9] B. B. Khlevnoy, N. J. Harrison, L. J. Rogers, D. F. Pollard, N. P. Fox, P. Sperfeld, J. Fischer, R. Friedrich, J. Metzdorf, J. Seidel, M. L. Samoylov, R. I. Stolyarevskaya, V. B. Khromchenko, S. A. Ogarev, and V. I. Sapritsky. Intercomparison of radiation temperature measurements over the temperature range from 1600 K to 3300 K. *Metrologia*, 40(1):S39–S44, 2003.

[10] K. Anhalt, J. Hartmann, J. Hollandt, G. Machin, D. Lowe, H. McEvoy, F. Sakuma, and L. Ma. Comparison of high temperature scales of the NMIJ

and the NPL with the scale of the PTB from 1300 K to 3200 K. In *Proceedings: TEMPMEKO 2004: 9th International Symposium on Temperature and Thermal Measurements in Industry and Science*, pages 1063–1068, 2004.

[11] M. Ojanen, K. Anhalt, J. Hartmann, S. Schiller, T. Weckström, P. Kärhä, M. Heinonen, and E. Ikonen. Comparison of the radiation temperature scales between MIKES and PTB. *Measurement*, 43(2):183–189, 2010.

[12] Commission Internationale de l'Éclairage. The basis of physical photometry. Technical Report 18.2, CIE Central Bureau, 1983.

[13] G. Wyszecki, W. R. Blevin, K. G. Kessler, and K. D. Mielenz. Principles governing photometry. BIPM Monographie 83/1. Bureau International des Poids et Mesures, 1983.

[14] L. P. Boivin, A. A. Gaertner, and D. S. Gignac. Realization of the new candela (1979) at NRC. *Metrologia*, 24(3):139–152, 1987.

[15] T. M. Goodman and P. J. Key. The NPL radiometric realization of the candela. *Metrologia*, 25(1):29–40, 1988.

[16] C. L Cromer, G. Eppeldauer, J. E. Hardis, T. C. Larason, Y. Ohno, and A. C. Parr. The NIST detector-based luminous intensity scale. *Journal of Research of the National Institute of Standards and Technology*, 101(2):109–132, 1996.

[17] W. Erb and G. Sauter. PTB network for realization and maintenance of the candela. *Metrologia*, 34(2):115–124, 1997.

[18] P. Toivanen, P. Kärhä, F. Manoochehri, and E. Ikonen. Realization of the unit of luminous intensity at the HUT. *Metrologia*, 37(2):131–140, 2000.

[19] S. M. Berman. Energy efficiency consequences of scotopic sensitivity. *Journal of the Illuminating Engineering Society*, 21(1):3–14, 1992.

[20] T. Uchida, Y. Zong, C. Miller, and Y. Ohno. A practical photometer for CIE performance based mesopic photometry system. Presented at CORM 2011: May 4–6, 2011.

[21] K. L. Cashdollar. Three-wavelength pyrometer for measuring flame temperatures. *Applied Optics*, 18(15):2595, 1979.

[22] P. B. Coates. Multi-Wavelength Pyrometry. *Metrologia*, 17(3):103–109, 1981.

[23] L. Sainiemi, K. Grigoras, I. Kassamakov, K. Hanhijärvi, J. Aaltonen, J. Fan, V. Saarela, E. Hæggström, and S. Franssila. Fabrication of thermal microbridge actuators and characterization of their electrical and mechanical responses. *Sensors and Actuators A: Physical*, 149(2):305–314, 2009.

[24] M. Blomberg, O. Rusanen, K. Keranen, and A. Lehto. A silicon microsystem-miniaturised infrared spectrometer. In *Proceedings of International Solid State Sensors and Actuators Conference (Transducers '97)*, volume 2, pages 1257–1258. IEEE, 1997.

[25] T. Corman, E. Kälvesten, M. Huiku, K. Weckström, P. T. Meriläinen, and G. Stemme. An optical IR-source and CO2-chamber system for CO2 measurements. *Journal of Microelectromechanical Systems*, 9(4):509–516, 2000.

[26] P. Ohlckers, A. M. Ferber, V. K. Dmitriev, and G. Kirpilenko. A photoacoustic gas sensing silicon microsystem. In *Transducers 2001*, pages 780–783, 2001.

[27] J. Tu, D. Howard, S. D. Collins, and R. L. Smith. Micromachined, silicon filament light source for spectrophotometric microsystems. *Applied Optics*, 42(13):2388–2397, 2003.

[28] J. Lee and W. P. King. Microcantilever hotplates: Design, fabrication, and characterization. *Sensors and Actuators A: Physical*, 136(1):291–298, 2007.

[29] P. Toivanen, J. Hovila, P. Kärhä, and E. Ikonen. Realizations of the units of luminance and spectral radiance at the HUT. *Metrologia*, 37(5):527–530, 2000.

[30] H. Yuasa, S. Ohya, S. Karasawa, K. Akimoto, S. Kodato, and K. Takahashi. Single crystal silicon micromachined pulsed infrared light source. In *Proceedings of International Solid State Sensors and Actuators Conference (Transducers '97)*, volume 2, pages 1271–1274. IEEE, 1997.

[31] C. H. Mastrangelo, J. H.-J. Yeh, and R. S. Muller. Electrical and optical characteristics of vacuum-sealed polysilicon microlamps. *IEEE Transactions on Electron Devices*, 39(6):1363–1375, 1992.

[32] P. Fürjes, Zs. Vizváry, M. Ádám, A. Morrissey, Cs. Dücső, and I. Bársony. Thermal investigation of micro-filament heaters. *Sensors and Actuators A: Physical*, 99(1-2):98–103, 2002.

[33] M. Born and E. Wolf. *Principles of optics*. Cambridge University Press, 1999.

[34] A. Haapalinna, P. Kärhä, and E. Ikonen. Spectral reflectance of silicon photodiodes. *Applied Optics*, 37(4):729–732, 1998.

[35] A. Haapalinna, F. Manoochehri, and E. Ikonen. High-accuracy measurement of specular spectral reflectance and transmittance. *Analytica Chimica Acta*, 380(2-3):317–325, 1999.

[36] I. H. Malitson. Interspecimen comparison of the refractive index of fused silica. *Journal of the Optical Society of America*, 55(10):1205–1209, 1965.

[37] G. E. Jellison and F. A. Modine. Optical functions of silicon at elevated temperatures. *Journal of Applied Physics*, 76(6):3758–3761, 1994.

[38] H. H. Li. Refractive index of silicon and germanium and its wavelength and temperature derivatives. *Journal of Physical and Chemical Reference Data*, 9(3):561–658, 1980.

[39] P. J. Timans. Emissivity of silicon at elevated temperatures. *Journal of Applied Physics*, 74(10):6353–6364, 1993.

[40] T. Satō. Spectral emissivity of silicon. *Japanese Journal of Applied Physics*, 6(3):339–347, 1967.

[41] B.-J. Lee, Z. Zhang, E. A. Early, D. P. DeWitt, and B. K. Tsai. Modeling radiative properties of silicon with coatings and comparison with reflectance measurements. *Journal of Thermophysics and Heat Transfer*, 19(4):558–565, 2005.

[42] M. A. Green and M. J. Keevers. Optical properties of intrinsic silicon at 300 K. *Progress in Photovoltaics: Research and Applications*, 3(3):189–192, 1995.

[43] G. Vuye, S. Fisson, V. Nguyen Van, Y. Wang, J. Rivory, and F. Abelès. Temperature dependence of the dielectric function of silicon using in situ spectroscopic ellipsometry. *Thin Solid Films*, 233(1-2):166–170, 1993.

[44] T. Uchida and Y. Ohno. Defining the visual adaptation field for mesopic photometry: Does surrounding luminance affect peripheral adaptation? *Lighting Research and Technology*, 46(5):520–533, 2014.

[45] M.S. Rea, J.D. Bullough, J.P. Freyssinier-Nova, and A. Bierman. A proposed unified system of photometry. *Lighting Research and Technology*, 36(2):85–111, 2004.

[46] T. Goodman, A. Forbes, H. Walkey, M. Eloholma, L. Halonen, J. Alferdinck, A. Freiding, P. Bodrogi, G. Varady, and A. Szalmas. Mesopic visual efficiency IV: a model with relevance to nighttime driving and other applications. *Lighting Research and Technology*, 39(4):365–392, 2007.

[47] K. Sagawa. Toward a CIE supplementary system of photometry: brightness at any level including mesopic vision. *Ophthalmic and Physiological Optics*, 26(3):240–245, 2006.

[48] A. Stockman and L. T. Sharpe. Into the twilight zone: the complexities of mesopic vision and luminous efficiency. *Ophthalmic and Physiological Optics*, 26(3):225–239, 2006.

[49] Commission Internationale de l'Éclairage. Recommended system for mesopic photometry based on visual performance. Technical Report 191, CIE Central Bureau, 2010.

[50] J. C. Zwinkels, E. Ikonen, N. P. Fox, G. Ulm, and M. L. Rastello. Photometry, radiometry and 'the candela': evolution in the classical and quantum world. *Metrologia*, 47(5):15–32, 2010.

[51] A. Ekrias, A.-M. Ylinen, M. Eloholma, and L. Halonen. Effects of pavement lightness and colour on road lighting performance. In *Proc. CIE Int. Symp. on Road Surface Photometric Characteristics: Measurement Systems and Results*, 2008.

[52] J. Mountford, G. Porrovecchio, M. Smid, and R. Smid. Development of a switched integrator amplifier for high-accuracy optical measurements. *Applied Optics*, 47(31):5821–5828, 2008.

Erratum

Publication IV

In figures 2, 3, 4, 5, 6 and 7: the units of luminance in the axis labels should read $\mathrm{cd \cdot m^{-2}}$, instead of $\mathrm{cd \cdot m^{-1}}$.

Publication I

M. Shpak, P. Kärhä, M. Ojanen, E. Ikonen and M. Heinonen, "Optical temperature measurement method for glowing microcomponents," *International Journal of Thermophysics* **31**, 1762–1770 (2010).

Publication II

M. Shpak, L. Sainiemi, M. Ojanen, P. Kärhä, M. Heinonen, S. Franssila and E. Ikonen, "Optical temperature measurements of silicon microbridge emitters," *Applied Optics* **49**, 1489–1493 (2010).

Optical temperature measurements of silicon microbridge emitters

Maksim Shpak,[1,*] Lauri Sainiemi,[2,3] Maija Ojanen,[1] Petri Kärhä,[1] Martti Heinonen,[4] Sami Franssila,[2] and Erkki Ikonen[1,4]

[1]Aalto University, Metrology Research Institute, P.O. Box 13000, FI-00076 Aalto, Finland

[2]Aalto University, Department of Materials Science and Engineering, P.O. Box 16200, FI-00076 Aalto, Finland

[3]Aalto University, Department of Micro and Nanosciences, P.O. Box 13000, FI-00076 Aalto, Finland

[4]Centre for Metrology and Accreditation, P.O. Box 9, FIN-02151 Espoo, Finland

*Corresponding author: maksim.shpak@tkk.fi

Received 26 August 2009; revised 15 February 2010; accepted 23 February 2010; posted 23 February 2010 (Doc. ID 116014); published 10 March 2010

Microbridges are miniature suspended structures fabricated in silicon. Passing a current through the microbridge can heat it up to the point of incandescence. A glowing microbridge can be used as a wide-band light source. This study presents a method for optical measurement of the temperature of a microbridge. Spectroscopic measurements of microbridges are optically challenging, because the multilayer structures cause interference effects. To determine the temperature from the emitted spectrum, the emissivity was modeled with thin-film Fresnel equations. Temperatures of 500–1100°C were obtained from the measured spectra at different levels of applied power. The range is limited by the sensitivity of the detectors at lower power levels and by the stability of the bridge at higher levels. Results of the optical measurements were compared with contact temperature measurements made with a microthermocouple in the same temperature range. The results of the two methods agree within 100 K.

OCIS codes: 230.6080, 230.4000, 120.6200, 120.6780, 310.6845.

1. Introduction

Microbridges are miniature suspended silicon structures that can be used as light sources in various spectrophotometric applications [1–4]. By passing an electrical current through the bridge, it can be rapidly heated up to the melting point of silicon (1410°C). Accurate measurement of the temperature of the bridge is difficult because of its small size. With a contact measurement, the risk to damage the bridge is high, and the heat escaping through the probe affects the results. Optical measurements are possible at temperatures where the emitted radiation is intense enough to be detected. In practice, the human eye sees that the bridge starts visibly glowing at 700–800°C, which is around the intrinsic temperature of silicon. This presents a problem for characterization of the microbridge, because thermal, electrical, and optical properties of silicon change rapidly at, near, and above intrinsic temperatures, where thermally generated charge carriers become dominant.

There are other studies of microbridges where the temperature has been determined by means of optical measurement [4–8]. However, a graybody assumption has been used in most studies. It is simple but leads to inaccuracies. We have experimentally determined the extinction coefficient of silicon in the temperature range of interest and included in the analysis interference effects from thin-film coatings.

0003-6935/10/091489-05$15.00/0

In this study, a method for optical temperature measurement of a microbridge was developed and tested. The method includes measurements of the visible and near-infrared spectra of a glowing microbridge with microscope optics coupled to a monochromator and calculation of the temperature with the help of Planck's radiation law. To describe the emissivity, a physical model was developed. This model relies on known optical properties of silicon and silicon dioxide as a function of temperature and doping concentration. The results obtained were compared with direct temperature measurements with a microthermocouple, and the data show good agreement within 100 K. Previous studies that have tried to combine information from optical and electrical measurements have not been able to reach overlapping temperature ranges [5], but have instead relied on interpolation of temperatures in the inaccessible temperature range of 800–1000°C, where the interesting peak of the resistance appears.

2. Microbridge Fabrication and Electrical Characteristics

The microbridges were fabricated on silicon-on-insulator (SOI) wafers, which had a 4 μm thick heavily boron-doped device layer and a 200 nm thick buried oxide layer. The bridges were formed in the device layer and released from the substrate by front-side sacrificial etching of the handle wafer. The air gap between the bridge and the handle wafer was around 15 μm. The resulting microbridges were fully covered with silicon dioxide. The top and the sidewalls of the bridges were covered by plasma-enhanced chemical-vapor-deposited silicon dioxide, and the bottom was protected by the buried oxide layer. The top and bottom layers were both 200 nm thick. Each anchor area had an aluminum contact pad, which was electrically isolated from the handle wafer by the buried oxide layer. The fabrication process is described in detail in [9].

The thickness and the doping level of the microbridge are defined by the device layer of the SOI wafer. This is an advantage over the diffusion-doped or the ion-implanted wafers, because the doping concentration is uniform and accurately controlled. A high level of doping concentration is desired to achieve low electrical resistivity. The boron doping in the device layer of the wafer was $5 \times 10^{18}\,\mathrm{cm}^{-3}$, which corresponds to the resistivity of 0.02 Ω cm. Figure 1 shows a schematic cross section and a scanning electron microscope image of the microbridge.

The conductivity of highly doped silicon has two distinct phases: extrinsic and intrinsic. At low temperatures, silicon is in the extrinsic phase, and the conductivity is determined by the mobility and concentration of the free carriers. As the mobility of the carriers decreases with higher temperatures, the resistance increases. At a certain temperature the thermally generated carriers start to dominate, and the resistance starts to decrease. This is the intrinsic phase. The resistance reaches its peak value at the intrinsic temperature, and for silicon with the doping concentration of $5 \times 10^{18}\,\mathrm{cm}^{-3}$, it is in the range of 650–900°C [9,10].

3. Optical Properties of a Microbridge

The size of the microbridge is 400 μm × 25 μm × 4 μm. Silicon is transparent in the infrared wavelength range at room temperature, but highly doped silicon becomes opaque at high temperatures. However, owing to the small thickness of the bridge, it can not be assumed to be fully opaque and to exhibit graybody properties. Also, the thicknesses of the different layers are comparable with the wavelengths of the emitted light and cause interference effects. Therefore, to accurately determine the temperature from the shape of the emitted spectrum, all mentioned effects on the emissivity must be taken into account.

Emissivity can be obtained from optical parameters of the materials, namely, the complex refractive indices. The total reflectivity and transmissivity of the stack of thin layers are calculated with Fresnel equations [11] and converted into emissivity by subtracting them from unity. Because the microbridge is a three-layer structure (SiO_2–Si–SiO_2), complex refractive indices are needed for both the highly doped silicon and the silicon dioxide at high temperatures. The real part of the refractive index for silicon was taken from Lee *et al.* [12], who suggested using a combination of expressions by Jellison and Modine [13] for wavelengths below 0.84 μm and the expression by Li [14] for wavelengths above 1.2 μm. The

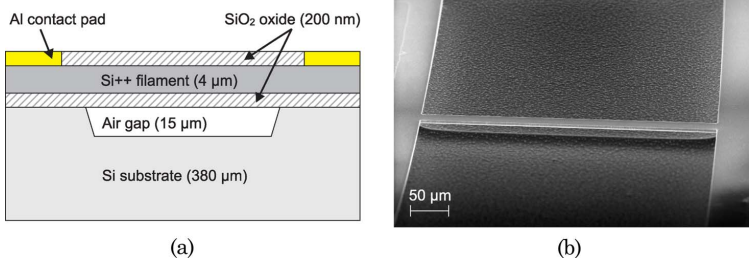

Fig. 1. (Color online) (a) Cross section schematic and (b) scanning electron microscope image of the microbridge.

refractive index for SiO_2 was taken from [15] and was assumed to be independent of the temperature.

In the wavelength range of interest, the extinction coefficient of silicon depends on absorption processes such as band-to-band transition and free-carrier absorption. The latter, in particular, is directly influenced by the doping concentration and has complicated behavior at high temperatures. While there have been many studies on the topic, most of them are confined to the temperatures below 800°C, and disagreement between the models increases with extrapolation to higher temperatures. For this reason, the extinction coefficient of the silicon used was determined experimentally from a SOI wafer by heating it in a furnace to a known temperature. The resulting emission spectrum was measured and fitted to match the theoretical prediction, using the extinction coefficients at different wavelengths as free parameters. As an example of the results, the polynomial describing the extinction coefficient at the temperature of 914°C is presented in Fig. 2. The extinction coefficient of SiO_2 was assumed to be negligible.

When the spectral emissivity $\epsilon(\lambda, T)$ as a function of temperature is known, the temperature of the measured object can be obtained with the help of Planck's radiation law. The measured signal is given by

$$S(\lambda, T) = B\epsilon(\lambda, T)\frac{2hc^2}{\lambda^5}\frac{1}{\exp\left(\frac{hc}{\lambda kT}\right) - 1}, \qquad (1)$$

where λ is the wavelength, h is the Planck constant, c is the speed of light, k is the Boltzmann constant, T is the temperature of the object, and B is a scaling factor due to the measurement geometry. The temperature is obtained from the wavelength dependence of the signal.

4. Experimental Setup

A. Contact Temperature Measurement

Contact temperature measurements were performed on an operating microbridge with a microthermocouple. The tip diameter was 13 μm. Measurements were taken starting from room temperature up to 1300°C, at which point the bridge failed. Excessive power input was required above 1000°C to compensate for losses via the thermocouple.

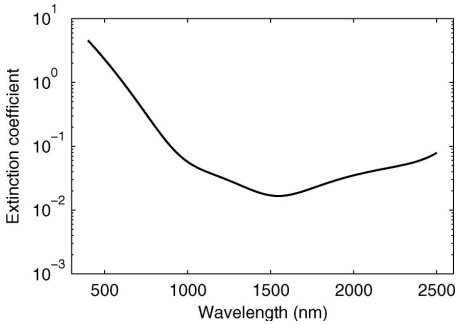

Fig. 2. Measured extinction coefficient for silicon at 914°C with a doping level of 5×10^{18} cm^{-3}.

B. Optical Measurements

The measurement setup is presented in Fig. 3. It consists of a double monochromator with a cooled photomultiplier tube for visible light detection and an InGaAs detector for the near-infrared. The optical configuration consists of a microscope objective with a nominal magnification of 10 and an aperture at the image plane to limit the measurement area to the center of the microbridge. Light passes through an optical chopper before entering the monochromator. The signal is detected with a lock-in amplifier. This setup permits measurements in the wavelength range from 250 to 1700 nm, with the 250–850 nm range covered by the photomultiplier tube and, the 850–1700 nm range by the InGaAs detector. The bandwidths were 2, 3, and 10 nm for the spectral ranges of 250–400, 400–850, and 850–1700 nm, respectively. The acquisition time at each wavelength setting was 1 s.

To calibrate the setup, an integrating sphere with four 50 W halogen lamps was used as a source. The microscope objective was focused at the exit port of the sphere. The sphere source itself was calibrated by comparing it with an irradiance standard lamp, using a spectoradiometer with diffuser optics. This calibration method ensures that the large field of view of the microscope objective is uniformly filled. The exit port of the integrating sphere can be considered a Lambertian source. Nonlinearity effects in the detectors are minimized by using a photodiode detector (InGaAs) and calibration signal levels close to the measured signal levels.

5. Results

Figure 4 shows measured spectra at three different temperatures. To fit Eq. (1) to the measured signal, multiple free parameters need to be adjusted. These parameters are the thicknesses of the three layers in the microbridge structure, the geometrical factor B, and the temperature T. Figure 5(a) shows the measured spectrum of the microbridge at the input power of 146 mW, and the modeled spectrum with

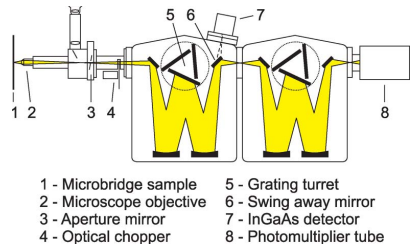

Fig. 3. (Color online) Configuration of the optical measurement setup.

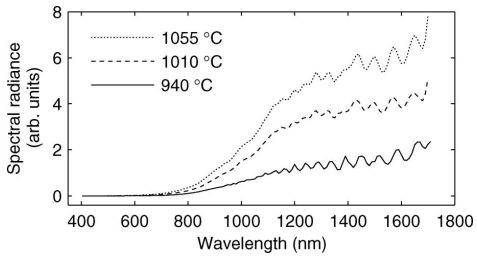

Fig. 4. Measured spectra of the microbridge at different temperatures.

$T = 940$°C. Figure 5(b) shows the measured and modeled spectral emissivities, calculated by dividing the spectrum of Fig. 5(a) by the spectral dependence of Planck's radiation law at 940°C. The modeled curve agrees well with the measured data. From Fig. 5(b), the interference patterns are evident. Slow oscillations, with the period of 100–300 nm, are caused by the interference in the top oxide layer, whereas the fast oscillations, with the period of less than 100 nm, are caused by interference in the silicon layer. The large dip in the emissivity from 1 to 2 μm is attributed to the transparency of the silicon layer because of the small thickness and the low extinction coefficient in that wavelength range (compare with Fig. 2).

When measuring at different supplied power levels, only the temperature parameter should need adjustment to achieve a good fit. In practice, however, the microbridge changes its shape owing to thermal expansion, arching upwards up to 10 μm. This affects the observed thicknesses of the layers

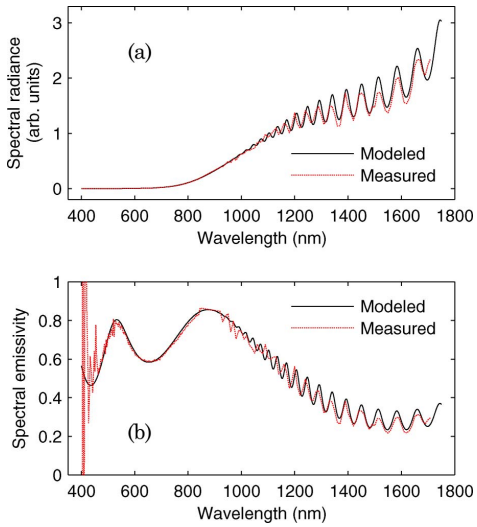

Fig. 5. (Color online) (a) Measured and modeled spectra and (b) corresponding emissivities.

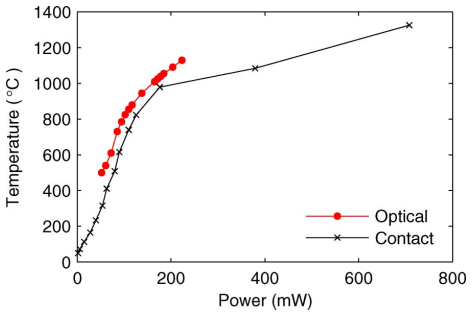

Fig. 6. (Color online) Comparison of measurement results obtained with contact and optical methods. Temperature is presented as a function of input power to the microbridge.

at the larger angles and weakens the amplitudes of the interference oscillations because of the effective averaging over the field of view of the microscope objective. Measurements were performed at various power levels, from 50 to 220 mW. At the lower end the limiting factor was the intensity of the emitted light, which could no longer be detected. At the upper end the microbridge becomes too unstable for the lengthy spectral scan to be performed, which takes approximately half an hour. At the same time, the voltage and current are monitored to determine the resistance of the microbridge.

Comparison of the contact measurements and the optical measurements is presented in Fig. 6, where measured temperatures are plotted as a function of the input power. The results follow a curve of the same shape, but there is an offset in the power levels. Since the measurements were performed on different samples, and with different sample holder and probe connection arrangements, this offset could be attributed to losses in the contact probes. Figure 7 shows normalized resistances of the bridge as a function of the temperature. There is a good agreement in the temperature dependence of the resistance obtained by the optical and contact measurements, and a good match of the temperatures of the peak

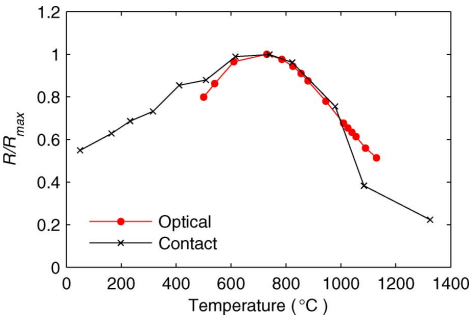

Fig. 7. (Color online) Comparison of measurement results obtained with contact and optical methods. Normalized resistances are presented as a function of temperature.

resistances. The deviation between the curves at temperatures above 1000°C is due to the heat escaping through the microthermocouple in the contact measurement. At temperatures below 600°C, the optical method becomes inaccurate, first, because of the low intensity of the emitted light and, second, because optical properties of the silicon change as it transforms from the intrinsic to the extrinsic phase.

6. Conclusions

This study shows that the temperature of a microbridge can be measured optically. However, a careful analysis of the measurement results is needed. Making a graybody assumption will result in a large error, especially if only a few wavelength points are measured. The emissivity model based on the thin-film equations allows determination of the temperature based on the shape of the measured spectrum and shows a good agreement between the predicted and the measured data. Measurements of the temperature performed by a direct contact with the microthermocouple agree within 100 K with the results obtained from the optical measurements, up to temperatures of 1000°C. For temperatures below 600°C, contact measurement is more accurate than optical because of the low intensity of the emitted light and the difficulty of modeling the emissivity.

The authors are grateful to Dr. Thua Weckström of the Centre for Metrology and Accreditation for providing assistance in measuring the extinction coefficient of silicon.

References

1. M. Blomberg, O. Rusanen, K. Keranen, and A. Lehto, "A silicon microsystem–miniaturised infrared spectrometer," in *International Conference on Solid State Sensors and Actuators. TRANSDUCERS '97* (IEEE, 1997), Vol. 2, pp. 1257–1258.
2. T. Corman, E. Kälvesten, M. Huiku, K. Weckström, P. T. Meriläinen, and G. Stemme, "An optical IR-source and CO_2-chamber system for CO_2 measurements," J. Microelectromech. Syst. **9**, 509–516 (2000).
3. P. Ohlckers, A. M. Ferber, V. K. Dmitriev, and G. Kirpilenko, "A photoacoustic gas sensing silicon microsystem," in *11th International Conference on Solid State Sensors and Actuators. Transducers '01* (Springer, 2001), Vol. 1, pp. 780–783.
4. J. Tu, D. Howard, S. D. Collins, and R. L. Smith, "Micromachined, silicon filament light source for spectrophotometric microsystems," Appl. Opt. **42**, 2388–2397 (2003).
5. P. Fürjes, Zs. Vizváry, M. Ádám, A. Morrissey, Cs. Dücső, and I. Bársony, "Thermal investigation of micro-filament heaters," Sens. Actuators A, Phys. **99**, 98–103 (2002).
6. H. Yuasa, S. Ohya, S. Karasawa, K. Akimoto, S. Kodato, and K. Takahashi, "Single crystal silicon micromachined pulsed infrared light source," in *International Conference on Solid State Sensors and Actuators. TRANSDUCERS '97* (IEEE, 1997), Vol. 2, pp. 1271–1274.
7. J. Lee and W. P. King, "Microcantilever hotplates: design, fabrication and characterization," Sens. Actuators A, Phys. **136**, 291–298 (2007).
8. C. H. Mastrangelo, J. H. Yeh, and R. S. Muller, "Electrical and optical characteristics of vacuum-sealed polysilicon microlamps," IEEE Trans. Electron. Devices **39**, 1363–1375 (1992).
9. L. Sainiemi, K. Grigoras, I. Kassamakov, K. Hanhijärvi, J. Aaltonen, J. Fan, V. Saarela, E. Hæggström, and S. Franssila, "Fabrication of thermal microbridge actuators and characterization of their electrical and mechanical responses," Sens. Actuators A, Phys. **149**, 305–314 (2009).
10. J. Kim, S. G. Kim, J. G. Koo, T. M. Roh, H. S. Park, and D. Y. Kim, "Characteristics of dynamic resistance in a heavily doped silicon semiconductor resistor," Int. J. Electron. **86**, 269–279 (1999).
11. M. Born and E. Wolf, *Principles of Optics* (Cambridge Univ. Press, 1999).
12. B. J. Lee, Z. M. Zhang, E. A. Early, D. P. DeWitt, and B. K. Tsai, "Modeling radiative properties of silicon with coatings and comparison with reflectance measurements," J. Thermophys. Heat Transfer **19**, 558–565 (2005).
13. G. E. Jellison, Jr., and F. A. Modine, "Optical functions of silicon at elevated temperatures," J. Appl. Phys. **76**, 3758–3761 (1994).
14. H. H. Li, "Refractive index of silicon and germanium and its wavelength and temperature derivatives," J. Phys. Chem. Ref. Data **9**, 561–601 (1980).
15. I. H. Malitson, "Interspecimen comparison of the refractive index of fused silica," J. Opt. Soc. Am. **55**, 1205–1209 (1965).

Publication III

M. Shpak, P. Kärhä, G. Porrovecchio, M. Smid and E. Ikonen, "Luminance meter for photopic and scotopic measurements in the mesopic range," *Measurement Science and Technology* **25**, 095001, 7 pages (2014).

IOP Publishing Measurement Science and Technology
Meas. Sci. Technol. **25** (2014) 095001 (7pp) doi:10.1088/0957-0233/25/9/095001

Luminance meter for photopic and scotopic measurements in the mesopic range

M Shpak[1,2], P Kärhä[2], G Porrovecchio[3], M Smid[3] and E Ikonen[1,2]

[1] Centre for Metrology and Accreditation (MIKES), PO Box 9, 02150 Espoo, Finland
[2] Metrology Research Institute, Aalto University, PO Box 13000, 00076 Aalto, Finland
[3] Czech Metrology Institute (CMI), V Botanice 4, 150 72 Prague, Czech Republic

E-mail: maksim.shpak@aalto.fi

Received 28 January 2014, revised 9 June 2014
Accepted for publication 11 June 2014
Published 22 July 2014

Abstract

This paper presents a design and realization of a dual-channel luminance meter for simultaneous measurement of luminance with photopic and scotopic weightings. Such measurements are useful in mesopic conditions, i.e. when the luminance is in the range of 0.005–5 cd m^{-2}. The instrument is a spot luminance meter with two spectrally weighted channels. The collected light is detected with silicon detectors and a computer-controlled dual-channel switched-integration amplifier. The instrument is characterized for relative spectral responsivity against a calibrated spectroradiometer using a radiance source based on an integrating sphere with input from a monochromator. An absolute luminance responsivity calibration is made against a sphere-based luminance standard at a level close to the high end of the mesopic range. The standard uncertainty in luminance responsivity calibration is 0.3% for the photopic channel and 0.6% for the scotopic channel. In addition, characterization measurements were carried out for the instrument's linearity, stray light sensitivity and polarization dependence. The results show very good noise performance, allowing fast measurements over the whole mesopic range. The noise equivalent power was measured to be approximately 20 fW $Hz^{-1/2}$, equal to a noise equivalent luminance of 30 μcd m^{-2} $Hz^{-1/2}$. Estimated uncertainty of measurements for typical light sources is 2.2% ($k = 2$) at the lowest luminance levels of the mesopic range.

Keywords: photometry, mesopic, luminance

(Some figures may appear in colour only in the online journal)

1. Introduction

Photometry provides tools to measure light in a way which correlates with human vision. This is achieved through the use of spectral luminous efficiency functions which simulate the visual response. The most widely used is the 2° photopic luminous efficiency function $V(\lambda)$ [1], applicable at relatively high light levels, where the visual response is formed by the cone cells in the retina. The photopic luminous efficiency function is applied, for example, in photometers with $V(\lambda)$ weighting that are used for the realization of the SI base unit candela [2–6].

At low light levels, only the rod cells in the eye are active, and the visual response is described by the scotopic luminous efficiency function $V'(\lambda)$ [1]. In the lighting conditions between the photopic and scotopic, both cone and rod cells are active, and the visual response changes depending on the level and the spectral distribution of the light to which the eye has adapted. This region is called mesopic, and the spectral luminous efficiency function $V_{mes}(\lambda)$ is calculated as a weighted average of $V(\lambda)$ and $V'(\lambda)$ in accordance with a recently published CIE recommendation [7].

Mesopic luminance can either be calculated from a measured radiance spectrum, or from separately measured photopic and scotopic luminances. It is also possible to combine relative spectral information with a photopic luminance measurement. Measurement of the radiance spectrum requires a spectroradiometer, an instrument considerably more complicated than filtered luminance meters. The need to disperse the measured light also reduces the light intensity incident on the detector, making this method less suitable for very low light

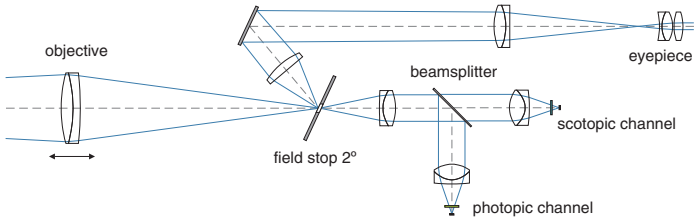

Figure 1. Optical layout of the luminance meter. Marginal optical rays are shown.

levels. Measurement of luminance over a 2° field of view at the low end of the mesopic range requires detection of total light power levels as low as 1 pW when using a filtered luminance meter. Even this poses challenges on the detection electronics, and with dispersing instruments, the situation is worse. It is therefore advantageous to use filtered instruments for luminance measurements in the mesopic and scotopic ranges.

In this work, we present a luminance meter capable of fast and simultaneous measurement of the photopic and scotopic luminance values. The instrument was characterized for spectral responsivity, linearity, noise performance, size of source effect and polarization. Estimated uncertainty at the lowest end of the mesopic range is 2.2%($k = 2$). A preliminary version of the instrument was presented at a CIE conference in 2013 [8], and since then was upgraded for an improved spectral matching in the scotopic channel and characterized in more detail for several correction factors. In addition, a detailed description is given of the advantages of measurements of the mesopic luminance with a double-channel luminance meter.

2. Mesopic photometry

According to the CIE recommendation [7], mesopic spectral luminous efficiency function $V_{\mathrm{mes}}(\lambda)$ is calculated as a linear combination of the photopic and scotopic luminous efficiency functions with the coefficients determined by the adaptation level of the observer. The mesopic luminous efficiency function is mathematically expressed as

$$V_{\mathrm{mes}}(\lambda) = \frac{1}{M(m)}[mV(\lambda) + (1 - m)V'(\lambda)], \qquad (1)$$

where $0 \leqslant m \leqslant 1$ is the adaptation level of the observer and $M(m)$ is a normalization function, such that $V_{\mathrm{mes}}(\lambda)$ has a maximum value of one. The adaptation level m is calculated from the adaptation luminance using an iterative algorithm or a look-up table [7]. The adaptation level assumes the value of one for adaptation luminance levels above 5 cd m^{-2} and the value of zero for adaptation luminance levels below 0.005 cd m^{-2}.

Mesopic luminance can be obtained by weighting the measured radiance spectrum by $V_{\mathrm{mes}}(\lambda)$ calculated using equation (1) at the required adaptation level m. Alternatively, photopic and scotopic luminance values can be combined to mesopic luminance

$$L_{\mathrm{mes}} = \frac{mL_{\mathrm{P}} + (1-m)\,L_{\mathrm{S}}\left(\frac{683}{1700}\right)}{m + (1-m)\left(\frac{683}{1700}\right)}, \qquad (2)$$

where L_{P} is the photopic luminance, L_{S} is the scotopic luminance, and 683/1700 is the normalization factor derived from the maxima of the photopic and scotopic luminous efficacies. The developed luminance meter uses measured L_{P} and L_{S} in equation (2) to obtain the mesopic luminance for a required value of m.

If the mesopic luminance determination is based on a measured radiance spectrum, a measurement error in the spectrum directly affects the scotopic luminance via the $V'(\lambda)$ weighted integration. This error source is, in principle, completely eliminated when the scotopic luminance is determined with a perfectly matched $V'(\lambda)$-filtered luminance meter. In practice, the spectral responsivity of the luminance meter deviates somewhat from the ideal $V'(\lambda)$, but as shown in section 4.3 the effect of this error source can remain relatively small, analogously to the spectral mismatch uncertainty in the realization of the candela using $V(\lambda)$-filtered photometers [2–6].

3. Luminance meter

The instrument developed is a spot luminance meter with separate filtered channels for the scotopic and photopic light detection. The optical layout of the instrument is presented in figure 1, and a photograph showing the internal components is presented in figure 2. The instrument consists of an objective lens which focuses the image onto a field stop corresponding to a 2° field of view, a beam splitter, and two detection channels with photopic and scotopic spectral weightings. The field stop also acts as a mirror which reflects the image around the measurement field into a viewfinder. Focusing is carried out by moving the objective lens. Spectral match of the channels' responsivities to the luminous efficiency functions $V(\lambda)$ and $V'(\lambda)$ has been optimized by selection of detectors, filters and optical coatings of the lenses. The beam splitter is a polka-dot type, chosen for its spectrally neutral optical characteristics.

Both measurement channels use Hamamatsu S1336-series silicon photodiodes with active areas of 3.6 mm × 3.6 mm and a custom-built dual-channel switched-integration amplifier (SIA) to measure the photocurrents [9]. The amplifier uses capacitors in the feedback loop instead of the traditionally used resistors of transimpedance amplifiers. The main advantage of SIA is improved noise performance at high gains, where the feedback resistor value would approach the shunt resistance of the detector. The amplifier is based on a Burr-Brown ACF2101 integrated circuit. It has a built-in 20-bit analog-to-digital converter and an 8-bit Freescale microcontroller which controls the switching timing and collects the data. Sensitivity of the amplifier is controlled by

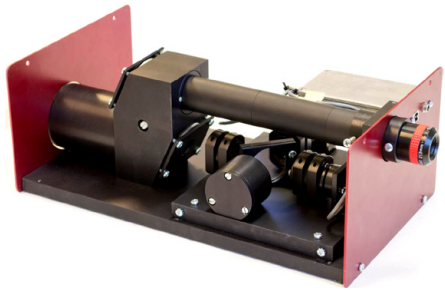

Figure 2. Internal view of the luminance meter. The outer dimensions are 370 × 210 × 140 mm^3.

selecting the feedback capacitor and the switching (integration) time. There are seven selectable values for the capacitor, and the integration time can be varied between 0.001 s and 0.8 s. The detection system has five decades of dynamic range. The detailed working principle of the amplifier is described in [9]. The instrument communicates via a USB connection with a measurement computer running LabView software.

4. Performance

4.1. Spectral responsivity

The instrument was calibrated for absolute responsivity in the photopic and scotopic channels using a wideband luminance source standard with a known photopic luminance and spectral radiance [10]. The color temperature of the source was 2856 K. The calibration took place at a photopic luminance level of 3 cd m^{-2}, close to the high end of the mesopic range. The standard uncertainty of the photopic luminance of the calibration source was 0.3%. The value includes the uncertainty of the scale realization and the additional uncertainty components due to measuring luminance levels lower than usual, such as background and noise. The scotopic luminance was calculated from the photopic luminance and the known relative spectral radiance. Uncertainty in the spectral radiance increased the obtainable standard uncertainty of the scotopic luminance value of the calibration source to 0.6%.

The relative spectral responsivities of both channels were measured using an integrating sphere as a source of monochromatic radiance. The measurement setup consisted of a halogen lamp source, a scanning monochromator, and optics directing the monochromator exit beam into the integrating sphere. The bandwidth of the monochromator was set to 2 nm, and the wavelength range of 380–780 nm was scanned with 2 nm steps. The spectral radiance at the output of the sphere at each wavelength setting of the monochromator was measured with a Konica–Minolta CS2000 spectroradiometer, the calibration of which is traceable to the spectral radiance scale of the Metrology Research Institute [10].

The normalized relative spectral responsivities $s^*_{\mathrm{rel}}(\lambda)$ of both channels are presented in figure 3. The corresponding luminous efficiency functions for photopic and scotopic

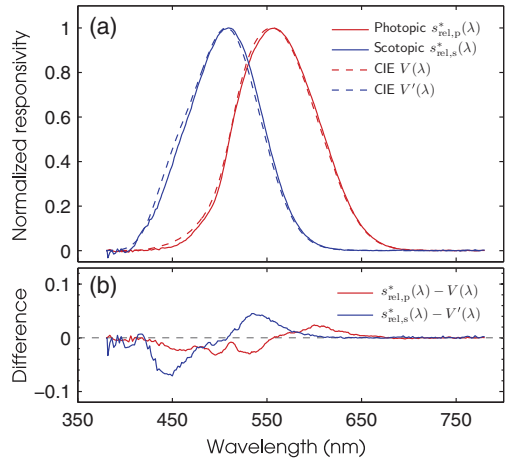

Figure 3. (*a*) Normalized relative spectral responsivities of the photopic and scotopic channels $s^*_{\mathrm{rel,p}}(\lambda)$ and $s^*_{\mathrm{rel,s}}(\lambda)$, and the corresponding CIE luminous efficiency functions $V(\lambda)$ and $V'(\lambda)$; (*b*) magnified differences $s^*_{\mathrm{rel,p}}(\lambda) - V(\lambda)$ and $s^*_{\mathrm{rel,s}}(\lambda) - V'(\lambda)$.

visions, as well as magnified differences from the measured values are also shown. Photometer spectral quality factor f'_1 for the photopic channel is 3.6%, and for the scotopic channel it is 6%. For a measurement of luminance from a typical white LED source, this mismatch causes a 1.3% error in the photopic channel and a 1.6% error in the scotopic channel, if spectral corrections are not applied. When correcting for the measured spectral responsivities and light source spectrum, the expectation values of the errors become zero with some uncertainties, which propagate through the uncertainties in the spectral responsivities of the instrument. We estimate that the standard uncertainties in the shapes of the spectral radiance responsivities are 1% throughout the visible wavelength range, calculated from the stray light properties of the reference spectroradiometer (CS2000) and the repeatability of the spectral responsivity calibrations.

4.2. Correction factors

The linearity of the luminance meter was measured at several levels in the luminance range of 0.0005–400 cd m^{-2}. Measurements were performed using a quasi-monochromatic luminance source based on an LED with a peak wavelength around 535 nm and an integrating sphere [11]. The intensity of the source was varied with an adjustable aperture at the entrance of the sphere. The luminance range was further extended by using several values of the driving current. Stability of the source was monitored with a detector mounted on the sphere, and the radiance spectrum was measured at the exit port of the sphere with a calibrated Konica-Minolta CS2000 spectroradiometer, used as the reference for linearity. The linearity of the CS2000 was verified relative to a linear silicon photodiode using a 536 nm mercury lamp line as the light source. The peak-to-peak deviation from linear behavior

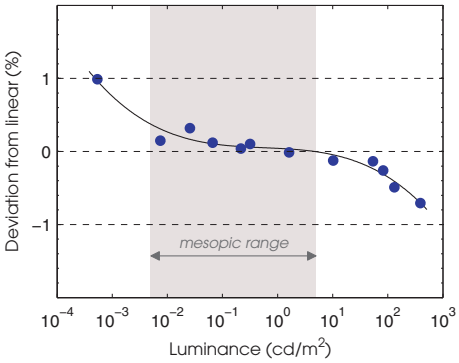

Figure 4. Deviation from the linear response as a function of measured photopic luminance is shown with dots. The solid line indicates the non-linearity correction.

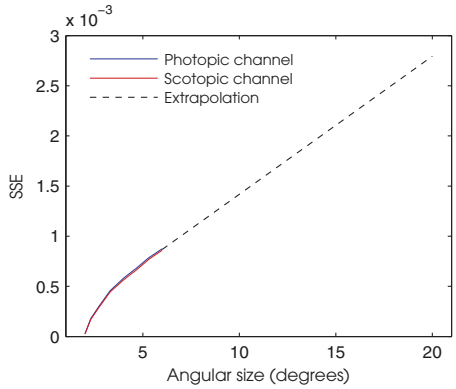

Figure 5. Measured size of source effect (SSE) for both channels in the range of 2–6° of the angular size of the target. A worst-case linear extrapolation to 20° is shown by the dashed line.

was less than 0.3% in the same power range as used in the linearity characterization of the luminance meter.

Results of the linearity measurements are presented in figure 4 as a function of the photopic luminance. The error in the luminance measurements caused by the nonlinearity is less than 2% in the full measured range, and less than 0.3% in the mesopic range of 0.005–5 cd m^{-2}, compared to the reference meter. Instrument components that affect the linearity of the system are the photodiodes and the amplifiers, thus similar results were obtained for both measurement channels. Results of nonlinearity measurements likely include the effects of stray light at the lowest scotopic levels. The effects of nonlinearity can be corrected in the measurement software.

Dark readings of both channels at the highest sensitivity setting and the highest integration time (0.8 s) correspond to the luminance level of 0.7 mcd m^{-2}. The relative standard deviation of the mean for the dark readings was 6%. This corresponds to less than 1% standard deviation of the mean at the luminance level of 0.005 cd m^{-2}, which is the lower limit of the mesopic range. The results can be expressed as a noise equivalent luminance of 30 μcd m^{-2} Hz$^{-1/2}$, or as a noise equivalent power (NEP) of 20 fW Hz$^{-1/2}$, which is double the value of the NEP specified for the photodiode alone. The noise performance can be further improved by numerical integration in the control software.

The size of the measured target affects the reading due to stray light entering the luminance meter from outside of the field of view. This source of error is known as the size of source effect (SSE). It was measured using an indirect method, with a variable aperture integrating sphere and central point obscuration [12]. Figure 5 shows the results of the measurements in the angular range of 2–6°, as well as linear extrapolation to 20°.

Due to the use of a beam splitter separating the measurement channels at 45° angle of incidence, the instrument is sensitive to the polarization of incident light. The polarization dependence was measured with an integrating sphere source, with an adjustable polarizer plate in front of the output port. The deviation in the readings between fully horizontally and fully vertically polarized light was found to be 18% for the photopic channel and 10% for the scotopic channel. There are ways to mostly eliminate the effects of polarization dependence, as described below.

The temperature dependence of the instrument was estimated from characteristics of the filters, photodiodes and switched-integration amplifier. The filters for the measurement channels have wavelength-dependent temperature coefficients of transmittance. The highest change is observed at around 520 nm, with a value of about 0.2%/°C [13]. Hamamatsu S1336 series photodiodes have negligible temperature coefficients of the responsivity in the visible wavelength range, but the dark current is highly temperature dependent, with a change of 15%/°C [14]. Temperature changes have an impact on the gain of the amplifier mainly due to the integration capacitor in the feedback loop. The typical specified temperature coefficient is 25 ppm/°C. The effects of these temperature coefficients are considered in detail in section 5.

4.3. Advantages of the dual-channel luminance meter

In mesopic and scotopic applications, one of the advantages of the dual-channel luminance meter over the photopic meter combined with the relative spectral information is the lower sensitivity to errors related to determination of the spectral distribution of the light source. When considering luminance measurement of a typical road surface, spectral reflectance of asphalt distorts the spectral shape of the source up to 20% [15]. Relative spectra of a typical white LED measured directly, and as reflected from asphalt, are presented in figure 6. If the change in the spectral distribution of the light source due to reflectance is not taken into account in calculation of the scotopic luminance based on measurements with a luminance meter with ideal $V(\lambda)$ weighting, the error in the obtained scotopic luminance is 6.5% in the case of the white LED. This error reduces to 1.1% with the use of our double-channel luminance meter even without correcting for deviation of $s^*_{\mathrm{rel,p}}(\lambda)$ and $s^*_{\mathrm{rel,s}}(\lambda)$ from $V(\lambda)$ and $V'(\lambda)$, respectively. In the case of

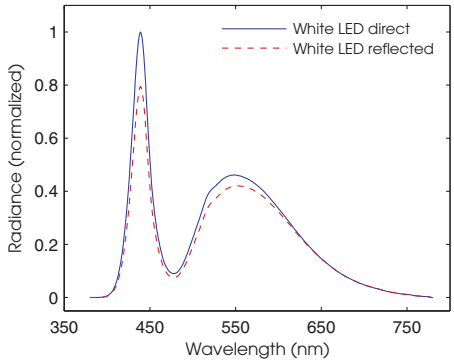

Figure 6. Relative radiance spectrum of a typical white LED, and calculated spectrum of the same LED reflected from an asphalt target. The reflectance of asphalt is 20% lower in the blue end of the visible spectrum as compared to the red wavelengths of 650–780 nm. The presented reflected spectrum is normalized to the direct spectrum at the red wavelength region.

a high pressure sodium (HPS) lamp the corresponding errors are 7.2% for the photopic luminance meter and 1.8% for the dual-channel luminance meter. Furthermore, if the spectral mismatch corrections are made to compensate for the spectral deviations of the dual-channel luminance meter's responsivities from the $V(\lambda)$ and $V'(\lambda)$ curves, the errors in the scotopic luminances caused by the reflectance of the surface reduce to 0.5% for white LED and to 0.4% for HPS.

5. Measurement uncertainty

The uncertainties of the luminance measurements with the presented instrument depend on the spectrum and the luminance level of the measured source, in addition to the environmental and geometrical factors. As an example, we present in table 1 uncertainty budgets for measurements of photopic and scotopic luminances of a target illuminated with the white LED spectrum of figure 6. The main uncertainty components are estimated separately for both channels and for three luminance levels: low end of the mesopic range, high end of the mesopic range, and one value higher in the photopic range.

The device is calibrated at the high end of the mesopic range (see section 4.1), and corrections due to non-linearity are applied elsewhere according to figure 4. The non-linearity corrections are estimated to have rectangular probability distributions and their standard uncertainty is calculated by taking half of the value of the applied correction and dividing it by $\sqrt{3}$. In addition, the uncertainty of the linearity of the reference instrument (CS2000), 0.15%, was added quadratically. The uncertainty of the non-linearity correction is naturally zero at the high mesopic range where the calibration takes place.

The repeatability component in table 1 includes uncertainties due to re-alignment. The uncertainty due to noise is based on the standard deviation of the dark signal readings with 1 s integration time.

Table 1. Uncertainty budgets for luminance measurements with the photopic and the scotopic channels, for three levels of (photopic) luminance. A target illuminated with the white LED spectrum of figure 6 is assumed. Uncertainty values are given in percentages.

	Photopic channel			Scotopic channel		
Luminance (photopic, cd m^{-2})	0.005	5	500	0.005	5	500
Calibration	0.30	0.30	0.30	0.60	0.60	0.60
Non-linearity correction	0.21	0.00	0.27	0.21	0.00	0.27
Repeatability	0.17	0.17	0.17	0.43	0.43	0.43
Noise (1 s int. time)	0.45	0.01	<0.01	0.45	0.01	<0.01
Spectral radiant responsivity	0.04	0.04	0.04	0.04	0.04	0.04
Source spectral shape	0.21	0.21	0.21	0.49	0.49	0.49
Size of source effect	0.22	0.22	0.22	0.22	0.22	0.22
Polarization	0.14	0.14	0.14	0.13	0.13	0.13
Temperature	0.24	0.24	0.24	0.32	0.32	0.32
Combined standard uncertainty	0.73	0.54	0.61	1.10	0.98	1.02
Expanded uncertainty ($k = 2$)	1.47	1.08	1.21	2.20	1.96	2.03

The spectral radiant responsivities of the channels have a standard uncertainty of 1%. This uncertainty propagates to the final results through the spectral mismatch correction factors of the channels. If we use a scenario, where deviations of ±1% are varied across different spectral ranges throughout the visible, we obtain a standard uncertainty of 0.04% for both channels. Uncertainty due to the spectral shape of the source is also introduced through the spectral mismatch correction uncertainty, calculated for the case of 20% deviation in the spectral distribution of the source, as shown in figure 6.

The size of source effect uncertainty is calculated as an error due to mismatch of the angular size of the luminance source between the measurement and calibration. The values are obtained by linear extrapolation of the SSE measurement results described in figure 5. The angular size of the calibration source is 4° and a 20° target is assumed.

The effects of polarization are a major source of error if not taken into account. In the case of fully horizontally or vertically polarized light, the deviations in readings from the equivalent luminance of non-polarized condition would be approximately 5% in the scotopic channel and 9% in the photopic channel. The actual error in the field application would depend on the angles of illumination and measurement, and on the type and condition of the measured surface. The effects of polarization can be compensated by taking an average of two measurements performed with the instrument rotated 0° and 90° around the optical axis. The associated uncertainty is then derived from the uncertainty in the angle of the instrument's orientation. The values in the uncertainty budget of table 1 are calculated for a 5° standard uncertainty in the angle of orientation and 20% difference between horizontal and vertical polarization components in the source luminance.

The uncertainty due to temperature variations takes into account errors caused by changes in filters' spectral transmittances. The scenario assumes a ±10 °C variation with respect to the calibration temperature. The effects due to responsivity change of the photodiodes and gain variation in the amplifiers are less than 0.01%. The change in the dark currents of

the photodiodes is compensated by the dark signal calibration prior to each measurement.

The combined expanded uncertainties are 1.08–1.47% for the photopic measurements, and 1.96–2.20% for the scotopic measurements, depending on the luminance level. It is worth noting that in a practical measurement in the field conditions, the spectrum of the source would typically not be known. Without spectral mismatch correction, the deviations of the channel responsivities from $V(\lambda)$ and $V'(\lambda)$ curves would in the case of the white LED source of figure 6 cause systematic errors of 1.3% and 1.6% to the photopic and scotopic luminances, respectively.

6. Conclusions

Measurement of mesopic luminance requires knowledge of the spectral characteristics of the light measured. This knowledge may be obtained either by measuring the spectral radiance, or by measuring separately the photopic and scotopic luminances. At the lower end of the range, it may not be practical to use spectrally resolving instruments due to the low amount of light available.

If the spectral distribution of the light is known, it is possible to calculate mesopic luminance for a certain adaptation level m based on a photopic luminance measurement alone. However, in many applications, it is unlikely that the measured surfaces have spectrally neutral reflectance characteristics. The spectral distribution would therefore need to be known separately for each measurement point. Use of a luminance meter with separate channels for photopic and scotopic weightings has clear advantages, reducing the uncertainty caused by spectral distribution deviation by as much as a factor of ten in some cases.

The developed instrument is a dual-channel spot luminance meter capable of simultaneous measurements of photopic and scotopic luminance levels covering the full mesopic range. The estimated expanded measurement uncertainty at the lowest end of the range is 2.2% ($k = 2$). Measured photometer spectral quality factors f_1' are 3.6% and 6% for the photopic and scotopic channels, respectively. Use of switched-integration amplifiers allows measurement of low light levels with good noise performance. At the lowest end of the mesopic range, a 0.5% standard deviation of the mean is attainable with less than 1 s of integration.

The instrument is capable of performing measurements in the mesopic range, and calculation of the mesopic luminance is possible as a function of the adaptation level m. However, at the moment there is no agreed way of measuring the adaptation level. Work is ongoing within the CIE to produce a recommendation for performing this measurement. Although currently this prevents using the instrument for true mesopic luminance measurements, it serves as a platform for further studies on the practical implementation of the mesopic system.

A future version of the dual-channel luminance meter is envisaged to include an adaptation level measurement capability in accordance with the upcoming CIE definition. In addition, the filters will be temperature stabilized and the polarization dependence reduced for more reliable outdoor operation. The latter can be achieved either by reducing the incidence angle of the light beam on the beam splitter or by measuring the horizontal and vertical polarization components separately with an electrically controlled polarizer. With these types of upgrades the instrument will support further development of mesopic photometry and offer reliable measurement of outdoor lighting conditions.

Acknowledgments

The authors acknowledge the Aalto Energy Efficiency Research Programme (project Light Energy—Efficient and Safe Traffic Environments) and European Metrology Research Programme (EMRP) project ENG05 ‘Metrology for Solid State Lighting’ for partially financing this work. The EMRP is jointly funded by the EMRP participating countries within EURAMET and the European Union. The authors also thank Anders Sjöberg for assisting with mechanical design and construction of the instrument.

References

[1] Commission Internationale de l’Éclairage 1983 The basis of physical photometry *CIE Technical Report* 18.2 CIE, Vienna
[2] Boivin L P, Gaertner A A and Gignac D S 1987 Realization of the New Candela (1979) at NRC *Metrologia* **24** 139–52
[3] Goodman T M and Key P J 1988 The NPL radiometric realization of the Candela *Metrologia* **25** 29–40
[4] Cromer C L, Eppeldauer G, Hardis J E, Larason T C, Ohno Y and Parr A C 1996 The NIST detector-based luminous intensity scale *J. Res. Natl Inst. Stand. Technol.* **101** 109–32
[5] Erb W and Sauter G 1997 PTB network for realization and maintenance of the candela *Metrologia* **34** 115–24
[6] Toivanen P, Kärhä P, Manoochehri F and Ikonen E 2000 Realization of the unit of luminous intensity at the HUT *Metrologia* **37** 131–40
[7] Commission Internationale de l'Éclairage 2010 Recommended system for mesopic photometry based on visual performance *CIE Technical Report* 191 CIE, Vienna
[8] Shpak M, Kärhä P, Porrovecchio G, Hirvonen J-M, Smid M and Ikonen E 2013 Characterized photopic-scotopic luminance meter for measurements in the mesopic range *Proc. CIE Centenary Conf. ‘Towards a New Century of Light’ (Paris, Apr. 2013)* pp 601–4
[9] Mountford A, Porrovecchio G, Smid M and Smid R 2008 Development of a switched integrator amplifier for high-accuracy optical measurements *Appl. Opt.* **47** 5821–8
[10] Toivanen P, Hovila J, Kärhä P and Ikonen E 2000 Realizations of the units of luminance and spectral radiance at the HUT *Metrologia* **37** 527–30
[11] Hirvonen J-M, Poikonen T, Vaskuri A, Kärhä P and Ikonen E 2013 Spectrally adjustable quasi-monochromatic radiance source based on LEDs and its application for measuring spectral responsivity of a luminance meter *Meas. Sci. Technol.* **24** 115201
[12] Machin G and Sergienko R 2001 A comparative study of size-of-source-effect (SSE) determination techniques *Proc. TEMPMEKO’01* **8** 155–60
[13] Kärhä P, Lassila A, Ludvigsen H, Manoochehri F, Fagerlund H and Ikonen E 1995 Optical power and transmittance

measurements and their use in detector-based realization of the luminous intensity scale *Opt. Eng.* **34** 2611–8

[14] Hamamatsu Photonics K K and Solid State Division 2014 *Si Photodiode S1336 Series* (Cat. No. KSPD1022E07)

[15] Ekrias A, Ylinen A, Eloholma M and Halonen L 2008 Effects of pavement lightness and colour on road lighting performance *Proc. CIE Int. Symp. on Road Surface Photometric Characteristics: Measurement Systems and Results (Torino, July 2008)*

Publication IV

M. Shpak, P. Kärhä and E. Ikonen, "Mathematical limitations of the CIE mesopic photometry system," *Lighting Research and Technology,* 11 pages, published online before print, DOI:10.1177/1477153515599436 (2015).

Lighting Res. Technol. 2015; **0**: 1–11

Mathematical limitations of the CIE mesopic photometry system

M Shpak MSc[a,b], **P Kärhä** PhD[b] and **E Ikonen** PhD[a,b]
[a]VTT Technical Research Centre of Finland Ltd, Centre for Metrology MIKES, Espoo, Finland
[b]Metrology Research Institute, Aalto University, Espoo, Finland

Received 3 May 2015; Revised 12 June 2015; Accepted 15 July 2015

The International Commission on Illumination (CIE) has published a recommended system for mesopic photometry based on visual performance. The system provides means for determining mesopic photometric values based on measuring the spectral composition and intensity of light. The system uses an iterative calculation method. We investigate the conditions under which this system is applicable and identify potential problems with the iterative method. We show that the system works well for the vast majority of lighting applications. However, it has non-convergence and discontinuity issues for sources with very high and very low values of scotopic-photopic ratio. A set of parameterised formulae is presented that approximates the mesopic model and provides a continuous, closed-form solution for the adaptation level in all lighting conditions.

1. Introduction

The human visual system relies on two distinct ways of detecting light. The visual response is formed by the cone photoreceptors at relatively high light levels and by the rod photoreceptors at low light levels. This is commonly referred to as day and night vision, or photopic and scotopic vision. The visual system has different spectral and angular responsivities in the two regimes, and thus photopic and scotopic measurements in photometry are also carried out with differently configured instruments. To perform photopic measurements, an instrument with a response matched to the photopic luminous efficiency function $V(\lambda)$ is needed, and for the scotopic measurement, the response has to be matched to the scotopic luminous efficiency function $V'(\lambda)$.[1] We have previously reported on our construction and characterisation of an instrument that can measure both photopic and scotopic luminance simultaneously.[2]

The spectral sensitivity of human vision can be purely scotopic, purely photopic or a combination of the two. Mesopic vision is the regime in which both cone and rod cells of the human eye are active, and the spectral sensitivity of the eye is dependent on its state of adaptation. Mesopic photometry aims to measure light in a way which correlates with the mesopic vision. The International Commission on Illumination (CIE) has published a recommendation for a performance-based mesopic photometry system CIE 191:2010.[3] The system provides a bridge between scotopic and photopic photometry. It has been developed with an emphasis on the visual performance in road and street lighting applications and is chiefly based on

Address for correspondence: M Shpak, Metrology Research Institute, Aalto University, Aalto FI-00076, Finland.
E-mail: maksim.shpak@aalto.fi

 10.1177/1477153515599436

two previously proposed systems: the unified system of photometry (USP)[4] and mesopic visual efficiency (MOVE).[5] Other systems for the mesopic range have been developed that use different criteria, such as brightness matching.[6] According to the CIE 191 system, mesopic luminous efficiency $V_{mes}(\lambda)$ is a linear combination of the photopic $V(\lambda)$ and scotopic $V'(\lambda)$ luminous efficiencies. The proportion in which the functions are combined is dictated by the adaptation level m, which is calculated from the mesopic luminance L_{mes} in the visual adaptation field, itself a function of m. This produces a recursive problem, and the CIE recommendation presents an iterative approach to solve both L_{mes} and m for given photopic and scotopic luminance values. The recommendation also provides tabulated values of the adaptation level m for typical combinations of photopic and scotopic luminances.

To perform a measurement in the mesopic range, the first step is to determine the adaptation level m from the photopic and scotopic luminances or from spectral measurements in the visual adaptation field. The mesopic luminous efficiency function $V_{mes}(\lambda)$ is then calculated with m and used to perform the final mesopic measurement. The measured mesopic value is only valid for the given adaptation level. For an instrument to be able to measure mesopic luminance, it needs to have a capacity of performing photopic/scotopic or spectral measurements in the adaptation field, to calculate adaptation level m and to apply m to weight the luminance measurement of the target with an appropriate $V_{mes}(\lambda)$.

In this paper, we investigate the CIE recommended mesopic model and the iterative algorithm within the full boundaries of the mesopic range. We show that discontinuities and non-convergence of the iterative algorithm exist at the opposite ends of the mesopic range with light sources exhibiting extreme, but still possible, scotopic-photopic ratios (S/P-ratio). The iterative algorithm may thus be impractical to implement in an automated system and may cause complications with uncertainty evaluation. The algorithm can be substituted by a formula that approximates it in a defined range, i.e. by parameterising the adaptation level with respect to the photopic and scotopic luminances. In addition to avoiding implementation of the iterative algorithm, a smooth formula guarantees continuity, avoids non-convergence and provides a straightforward way of calculating uncertainty propagation via partial derivatives.

2. S/P-ratio

A light source will produce different luminance values, depending on whether it is evaluated with a photopic or a scotopic spectral weighting. The ratio of the scotopic luminance to the photopic luminance obtained for the same radiance spectrum is called the scotopic/photopic ratio (S/P-ratio, R_{sp}).[7] Photopic luminous efficiency function is defined in the 360–830 nm range, and scotopic luminous efficiency function in a slightly narrower 380–780 nm range. All defined values for both functions in their respective ranges are positive.[1] Using values in the overlapping range, theoretical limits for the S/P-ratio can be obtained. Figure 1 presents photopic and scotopic luminous efficacy functions at the 380–780 nm range, and S/P-ratios for monochromatic light, where the range of possible S/P-ratios is approximately $0.01 \leq R_{sp} \leq 73$. The limiting values can only be achieved with monochromatic light. For light with spectral components in the 360–380 nm or 780–830 nm ranges, the S/P-ratio can also get values between 0 and 0.01. Typical light sources used for lighting have broad spectra, and their S/P-ratios are far from the limit values.

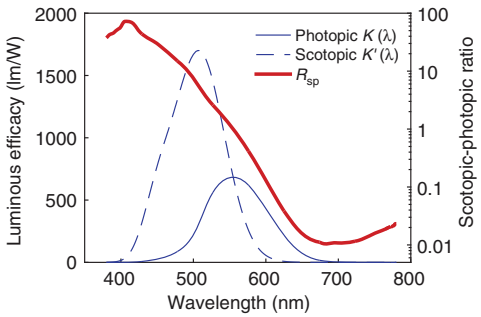

Figure 1 Photopic $K(\lambda)$ (thin solid blue line) and scotopic $K'(\lambda)$ (thin dashed blue line) spectral luminous efficacies and the S/P-ratio R_{sp} (thick red line) produced by monochromatic light

Table 1 Typical light sources and their S/P-ratio values

Light source	R_{sp}
Low pressure sodium	0.23
High pressure sodium	0.4
Mercury vapour lamp	0.8
Incandescent	1.41
Quartz halogen	1.5
Fluorescent	1.5–2.4
Cool white LED	2.3
LED – red (635 nm)	0.06
LED – blue (470 nm)	14.3
LED – royal blue (450 nm)	28
Diode laser – red (650 nm)	0.016
Diode laser – blue (445 nm)	32

LED: light emitting diodes; S/P-ratio: scotopic-photopic ratio

Table 1 shows S/P-ratios for several typical sources used in lighting, as well as some common quasi-monochromatic sources that produce extreme S/P-ratio values.

The mesopic system presented in CIE 191[3] was developed for use with moderate S/P-ratio values and may not correlate well with visual performance under lighting with extreme S/P-ratio values. Although unlikely, the lighting conditions which exhibit extreme S/P-ratios are not impossible. For example, red light-emitting diodes (LEDs) are used in traffic lights and car tail lights, which can dominate the adaptation field when no other light sources are present. Red LED flashlights are sometimes used specifically for their low S/P-ratio, to avoid losing scotopic adaptation and to aid with the night vision. On the other hand, blue LEDs are common in decorative lighting, advertisement signs and car interiors.

3. Mesopic photometry system

3.1. Definition

In accordance with the CIE 191 recommended system for mesopic photometry,[3] the mesopic spectral luminous efficiency function $V_{mes}(\lambda)$ is calculated as a linear combination of the photopic spectral luminous efficiency function $V(\lambda)$ and the scotopic spectral luminous efficiency function $V'(\lambda)$ as

$$V_{mes}(\lambda) = \frac{1}{M(m)}[mV(\lambda) + (1-m)V'(\lambda)] \quad (1)$$

where $0 \leq m \leq 1$ is the adaptation level of the observer and $M(m)$ is the normalisation function, such that $V_{mes}(\lambda)$ attains a maximum value of 1. Mesopic luminance L_{mes} is obtained by weighting the spectral radiance $L_e(\lambda)$ with the mesopic luminous efficiency function $V_{mes}(\lambda)$ and by integrating over the visible wavelength range

$$L_{mes} = \frac{K_{cd}}{V_{mes}(\lambda_0)} \int V_{mes}(\lambda) L_e(\lambda) d\lambda \quad (2)$$

where $\lambda_0 \approx 555.016$ nm is the wavelength in standard air at which the SI unit of candela is defined[1] and $K_{cd} = 683$ lm/W is the luminous efficacy of monochromatic radiation at λ_0.[8] Combining equations (1) and (2), the mesopic luminance L_{mes} can be expressed as a weighted sum of the photopic luminance L_p and the scotopic luminance L_s

$$L_{\mathrm{mes}} = \frac{mL_{\mathrm{p}} + (1-m)L_{\mathrm{s}}V'(\lambda_0)}{m + (1-m)V'(\lambda_0)} \tag{3}$$

where $V'(\lambda_0) \approx 0.40175$ is the value of the scotopic luminous efficiency functions at λ_0.[9] A detailed derivation of equation (3) is given in the appendix.

The value of the adaptation level m is calculated from the mesopic luminance L_{mes} in the visual adaptation field and both values are solved using an iterative algorithm. The iteration is carried out as

$$m_0 = 0.5 \tag{4}$$

$$L_{\mathrm{mes},n} = \frac{m_{n-1}L_p + (1-m_{n-1})L_sV'(\lambda_0)}{m_{n-1} + (1-m_{n-1})V'(\lambda_0)} \tag{5}$$

$$m_n = a + b\log_{10}\left(L_{\mathrm{mes},\,n}/L_0\right), \quad \text{for } 0 \le m_n \le 1 \tag{6}$$

where $L_0 = 1$ cd·m^{-2} and values for parameters a and b are

$$a = 1 - 1/3\log_{10}(5) \tag{7}$$

$$b = 1/3 \tag{8}$$

The iteration with equations (5) and (6) continues until the values of L_{mes} and m have converged to an acceptable precision level. It is also stated in the recommendation that the adaptation level gets a value of $m = 1$ for mesopic luminance values $L_{\mathrm{mes}} \ge 5.0$ cd·m^{-2} and a value of $m = 0$ for mesopic luminance values $L_{\mathrm{mes}} \le 0.005$ cd·m^{-2}. These boundary conditions were used to derive exact values for a and b in equations (7) and (8), respectively.

In the CIE 191 recommendation approximate values of $a = 0.7670$ and $b = 0.3334$ are given for equation (6). However, it should be noted that using these approximate values it is possible to obtain both $m_n < 0$ and $m_n > 1$ from equation (6) in certain conditions, where $L_{\mathrm{mes,n}}$ is very close to the limits of the mesopic range. For example, by using $L_{\mathrm{mes,n}} = 0.005001$ cd·m^{-2}, equation (6) produces $m_n \approx -0.00013$; and by using $L_{\mathrm{mes,n}} = 4.999$ cd·m^{-2}, it produces $m_n \approx 1.0000007$. Although these values are very close to the limits, these conditions are undefined in the recommendation and will result in a mathematical error during the next iteration step, should the algorithm be implemented in an automated system. For all analyses in this paper the exact values for a and b in equations (7) and (8) were used, which keeps m in the defined range.

3.2. Visualisation of the mesopic region

The entire mesopic region can be described as a three-dimensional graph, where the mesopic luminance is expressed as a function of photopic and scotopic luminances as $L_{\mathrm{mes}}(L_{\mathrm{p}}, L_{\mathrm{s}})$. Similarly, the mesopic range can be presented as the adaptation value $m(L_{\mathrm{p}}, L_{\mathrm{s}})$, as shown in Figure 2(a). Because only certain ratios of L_{p} and L_{s} are possible for light sources emitting between 380 nm and 780 nm ($0.01 \le R_{\mathrm{sp}} \le 73$), it might be beneficial to plot the mesopic space as a function of the photopic luminance and the S/P-ratio as $m(L_{\mathrm{p}}, R_{\mathrm{sp}})$ instead. This preserves the rectangular shape of the allowed value space and helps with parameterisation. Values of L_{p} and R_{sp} that delimit the mesopic range are shown in Figure 2(b). For both graphs in Figure 2, the shaded areas are within the allowed S/P-ratio range, $m = 0$ is the scotopic end of the range and $m = 1$ is the photopic end.

3.3. High S/P-ratios

For a light source with high S/P-ratio and photopic luminance values of L_{p} close to 5 cd·m^{-2}, the iterative algorithm may not converge. The lower limit for the S/P-ratio where non-convergence may appear is approximately 17. A plot illustrating the area of non-convergence is presented in Figure 3 as $L_{\mathrm{mes}}(L_{\mathrm{p}}, R_{\mathrm{sp}})$. The plot area includes the whole mesopic region, as in the plots of Figure 2, but on linear scales. Limits

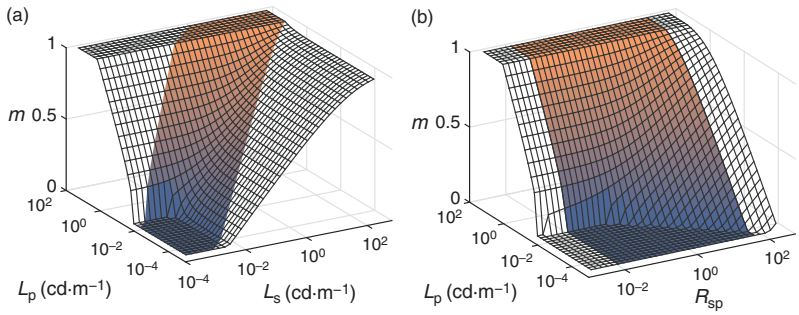

Figure 2 Adaptation level m as a function of (a) L_p and L_s and (b) L_p and R_{sp}. The non-shaded areas represent S/P-ratios that are outside the mathematically possible range for light sources emitting between 380 nm and 780 nm

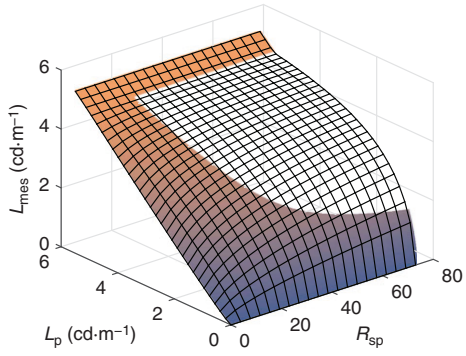

Figure 3 Mesopic luminance as a function of L_p and R_{sp} on linear scales. The iterative model does not converge in the non-shaded area

of the area of non-convergence were found by applying the iterative algorithm for every combination of L_p and R_{sp} in the region.

As an example of non-convergence, iteration steps with values of $L_p = 4\,\text{cd}\cdot\text{m}^{-2}$ and $L_s = 80\,\text{cd}\cdot\text{m}^{-2}$ (i.e. $R_{sp} = 20$) are presented in Table 2. The non-convergence arises from the fact that the scotopic component is sufficiently high to push the value of $L_{\text{mes},n}$ over the 5 $\text{cd}\cdot\text{m}^{-2}$ limit in step 3 (equation (5)), so that m_n gets limited to the value of 1 (equation (6)). In the next step, $L_{\text{mes},n+1}$ becomes equal to L_p, which drops m_{n+1} back to the value that overemphasises the scotopic portion. Values in step 4 are equal to the values in step 2; thus, the pattern repeats infinitely without converging. However, the non-convergence is caused by the mathematical shortcomings of the iterative approach, and not by a physiological phenomenon.

It is possible to use a more robust algorithm to find a value of m, which combines L_p and L_s in a ratio sufficient to stay in the mesopic range. This can be achieved by solving equations (5) and (6) numerically as a pair of equations with $m_n = m_{n-1} = m$. For the example above, the correct value of the adaptation level is $m \approx 0.9843$, which produces a value for mesopic luminance of $L_{\text{mes}} \approx 4.4850\,\text{cd}\cdot\text{m}^{-2}$. The values in the non-shaded area of Figure 3 were obtained using a non-linear solving method, specifically an 'fminsearch' function of MATLAB R2014b.

3.4. Low luminance values

At the low end of the mesopic range with $R_{sp} < 1$, the iterative model exhibits discontinuity. The number of iterations needed to achieve convergence is rising closer to the edge of the discontinuity. The discontinuity on the $L_{\text{mes}}(L_p, R_{sp})$ plot is shown in Figure 4. The heat map at the bottom of Figure 4 shows the increase in the iteration steps

Table 2 Iteration steps n for high S/P-ratio non-convergence ($R_{sp} = 20$). Values in parentheses are results of equation (6) before limiting m to the allowed range

n	1	2	3	4	5
m_{n-1}	0.5	1	0.9677	1	0.9677
$L_{mes,n}$	25.783	4	5.006	4	5.006
m_n	1 (1.24)	0.9677	1 (1.0002)	0.9677	1 (1.0002)

S/P-ratio: Scotopic-photopic ratio

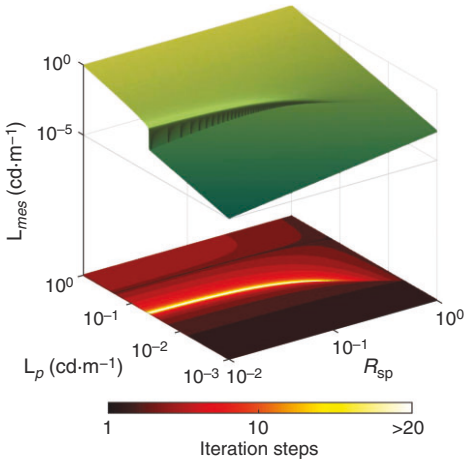

Figure 4 Discontinuity at the low edge of the mesopic range. The number of iterations needed to achieve convergence is shown as the heat map under the surface graph

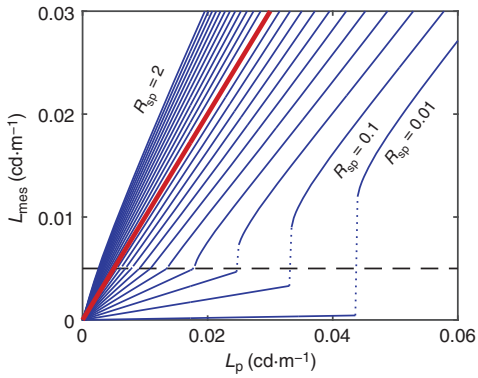

Figure 5 Transition between the scotopic and the mesopic range for 24 values of the S/P-ratio, where discontinuity is shown with dotted lines. The thick red line indicates the S/P-ratio of $R_{sp} = 1$, and the horizontal dashed line is the lower limit of the mesopic range

required to achieve convergence at the level of $m_n - m_{n-1} \leq 10^{-4}$.

Another way to look at the discontinuity is that for a given S/P-ratio, there is a transition on the $L_{mes}(L_p)$ curve, where m suddenly changes from zero to a positive value with increasing luminance. This transition is presented in Figure 5 for several values of R_{sp}. The discontinuity in the mesopic luminance with the smooth increase of light intensity is likely not a representation of a physiological phenomenon, but an artefact of the CIE mesopic model, which forces the response to be purely scotopic for L_{mes} values below 0.005 cd·m^{-2}, despite the low S/P-ratio. The problem of discontinuity is considerably more difficult to deal with as compared with the problem of non-convergence.

4. Parameterisation

Here, we present one possible way to parameterise the mesopic model to allow calculation of the adaptation level m from the measured photopic and scotopic luminance values.

One of the goals set for the parameterised formula is to ensure continuity in the transition from scotopic to mesopic conditions with low S/P-ratios. This necessarily deviates from the CIE 191 recommendation, which states that for mesopic luminance values $L_{\mathrm{mes}} < 0.005\,\mathrm{cd{\cdot}m^{-2}}$, adaptation level m is zero and the vision is purely scotopic. This effectively removes the contribution of the photopic luminance from consideration, even if its value is high, as can be the case with light that has a low S/P-ratio. Our modified requirement is that m is equal to zero only when both photopic and scotopic luminances are below $0.005\,\mathrm{cd{\cdot}m^{-2}}$, which allows for L_{mes} values below $0.005\,\mathrm{cd{\cdot}m^{-2}}$ with sufficiently low R_{sp} values.

The parameterised formula takes the photopic luminance L_{p} and the S/P-ratio R_{sp} as arguments, where $R_{\mathrm{sp}} = L_{\mathrm{s}}/L_{\mathrm{p}}$. The mesopic region is parameterised separately for $R_{\mathrm{sp}} \le 1$ and $R_{\mathrm{sp}} > 1$. In total, four possible conditions are defined, where $L_1 = 0.005\,\mathrm{cd{\cdot}m^{-2}}$ and $L_2 = 5\,\mathrm{cd{\cdot}m^{-2}}$:

1) When $L_{\mathrm{p}} \le L_1$ and $R_{\mathrm{sp}} \le 1$, the value of m is always 0.
2) When $L_{\mathrm{p}} \ge L_2$, the value of m is always 1.
3) When $L_1 < L_{\mathrm{p}} < L_2$ and $R_{\mathrm{sp}} \le 1$, the value of m is given by

$$\begin{aligned} m = {} & 1/3 \cdot R_{\mathrm{sp}} \cdot \log_{10}(L_{\mathrm{p}}/L_1) \\ & + \alpha \cdot (R_{\mathrm{sp}} - 1) \cdot \log_{10}^2[\log_{10}(L_{\mathrm{p}}/L_1) + 1] \\ & + \beta \cdot (R_{\mathrm{sp}} - 1) \cdot \log_{10}^3[\log_{10}(L_{\mathrm{p}}/L_1) + 1] \\ & + \gamma \cdot (R_{\mathrm{sp}} - 1)^4 \cdot (L_{\mathrm{p}} - L_1)^2 \\ & \cdot e^{-4\log_{10}^2(L_{\mathrm{p}}/L_1)} \end{aligned} \tag{9}$$

where the fitted coefficients are $\beta = 0.28$, $\gamma = -1300\ \mathrm{m^4{\cdot}cd^{-2}}$, and α is defined in terms of β with the equation

$$\alpha = \frac{1 + \beta \cdot \log_{10}^3(4)}{\log_{10}^2(4)} \approx -2.88 \tag{10}$$

4) When $L_{\mathrm{p}} < L_2$ and $R_{\mathrm{sp}} > 1$, the value of m is given by

$$\begin{aligned} m = {} & \left(1/3 + p_{11}\log_{10}R_{\mathrm{sp}} + p_{12}\log_{10}^2 R_{\mathrm{sp}} \right. \\ & \left. + p_{13}\log_{10}^3 R_{\mathrm{sp}}\right) \cdot \log_{10}\left(\frac{L_{\mathrm{p}}R_{\mathrm{sp}}}{L_1}\right) \\ & + \left(p_{21}\log_{10}R_{\mathrm{sp}} + p_{22}\log_{10}^2 R_{\mathrm{sp}}\right. \\ & \left. + p_{23}\log_{10}^3 R_{\mathrm{sp}}\right) \cdot \log_{10}^2\left(\frac{L_{\mathrm{p}}R_{\mathrm{sp}}}{L_1}\right) \\ & + \left(p_{31}\log_{10}R_{\mathrm{sp}} + p_{32}\log_{10}^2 R_{\mathrm{sp}}\right. \\ & \left. + p_{33}\log_{10}^3 R_{\mathrm{sp}}\right) \cdot \log_{10}^3\left(\frac{L_{\mathrm{p}}R_{\mathrm{sp}}}{L_1}\right) \end{aligned} \tag{11}$$

where p_{ij} are the fitted coefficients, listed in Table 3. In all cases m is larger than zero. In conditions where equation (11) produces negative values, m should be assigned a value of 0. Equation (11) aims to model the CIE 191 system with minimal deviation, but the numerical solution of equations (5) and (6) could be used in condition 4 instead. Equations (9) to (11) and their coefficients were obtained by trial and error, with the goal of minimising deviations from the values obtained by the iterative CIE 191 method.

Figure 6(a) shows the parameterised adaptation level m as a function of L_{p} and R_{sp}, and Figure 6(b) shows the low end of the mesopic luminance L_{mes} as a function of L_{p} and R_{sp}, where the CIE 191 model exhibits discontinuity. The value of L_{mes} is calculated from the modelled values of m by equation (3). It should be noted, that with the parameterised model, it is no longer possible to calculate values of m from the mesopic luminance L_{mes} by equation (6), as the

Table 3 Coefficients for equation (11)

$p_{11} = -0.2176$	$p_{12} = 0.1974$	$p_{13} = -0.06187$
$p_{21} = 0.04633$	$p_{22} = -0.06869$	$p_{23} = 0.02813$
$p_{31} = -0.004613$	$p_{32} = 0.006027$	$p_{33} = -0.0029$

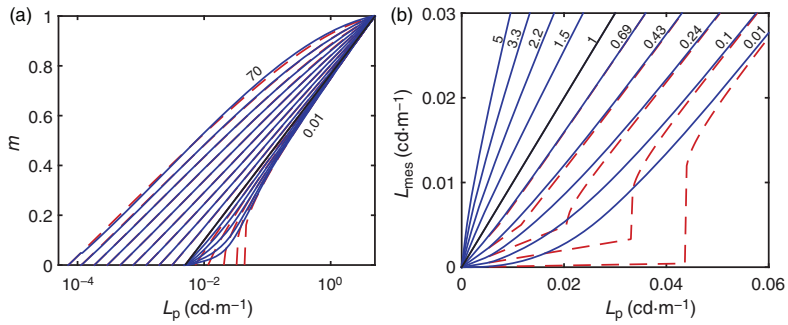

Figure 6 (a) Adaptation level m as a function of L_p for 15 values of R_{sp} between 0.01 and 70, obtained with the parameterised model. (b) Mesopic luminance L_{mes} as a function of L_p for 10 values of R_{sp} between 0.01 and 5, calculated from m. Solid lines are calculated from the parameterised values of m, and red dashed lines are calculated using the CIE iterative algorithm or solving the pair of equations (5) and (6). The numbers next to the curves indicate their R_{sp} values

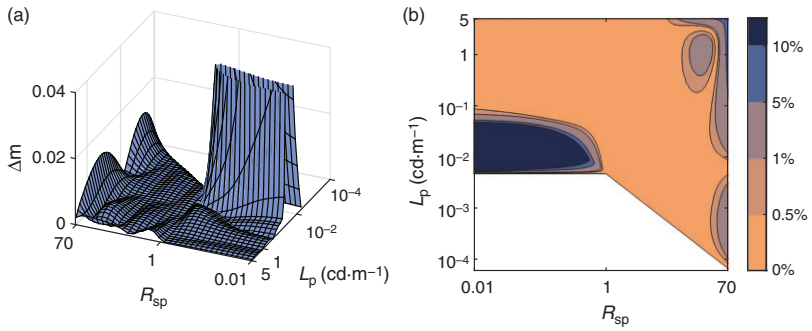

Figure 7 (a) Absolute difference Δm between the adaptation levels obtained from the CIE model and from the parameterised model, as a function of L_p and R_{sp}. (b) Relative deviations of calculated values of L_{mes} caused by the differences in values of m, as a function of L_p and R_{sp}

model does not reproduce the CIE 191 recommendation values exactly, and allows $L_{mes} < 0.005\,cd{\cdot}m^{-2}$.

The absolute difference of the parameterised adaptation level m from the CIE 191 recommendation is shown in Figure 7(a) for the full mesopic range. The effect of this difference on the calculated values of L_{mes} is shown in Figure 7(b). For most of the useful mesopic range, the difference in m is below 0.005, and the effect of this difference on L_{mes} is below 0.5%. For $R_{sp} > 40$, the difference between the CIE model and equation (11) is less than 0.013 for m, and the effect on L_{mes} is less than 10%. For $R_{sp} < 1$, and for luminance values of $L_p < 0.1\,cd{\cdot}m^{-2}$, the differences increase due to the discontinuity in the CIE model.

5. Conclusions

In this work, we have investigated the mesopic photometry model presented in the

CIE 191 recommendation, from the point of view of its implementation in automated measurement instruments. The recommendation presents an algorithm for calculation of the adaptation level m from the measured values of photopic and scotopic luminances L_p and L_s. The algorithm relies on an iterative calculation process. For the vast majority of light sources and lighting applications the model and its iterative algorithm work well, but it has, in principle, discontinuity and non-convergence problems at the extreme ends of the mesopic range. The iterative model should be used with caution where $R_{sp} > 17$, and with low luminance values, i.e. $L_{mes} < 0.015\,cd{\cdot}m^{-2}$ when $R_{sp} < 1$.

With a source spectrum of very high S/P-ratio, the iterative algorithm may be unable to find a solution, and ends up switching between two distinct values of L_{mes} indefinitely. Conditions where this is possible are limited to S/P-ratios over 17. The solution for m can nevertheless be found by numerically solving equations (5) and (6).

At the low end of the mesopic range, the transition between scotopic and mesopic responses is not smooth for values of the S/P-ratio smaller than one. The discontinuity is more pronounced with smaller S/P-ratios. The main reason for the discontinuity is the strict limit for the mesopic range, where any luminance with a mesopic value smaller than $0.005\,cd{\cdot}m^{-2}$ is considered purely scotopic, irrespective of the S/P-ratio. So, in lighting conditions with very high photopic and very low scotopic content, and smoothly increasing intensity, luminance will undergo a rapid increase when passing the $0.005\,cd{\cdot}m^{-2}$ limit, as it starts to take the photopic component into account. For values close to the edge of the scotopic-mesopic transition, the solving algorithm may require a high number of iterations to reach a solution.

The goal set for development of the mesopic system that resulted in the CIE 191 recommendation was to produce a model that describes visual performance. In this case, visual performance is described by such factors as detectability and reaction time. The resulting model relies on empirical observations rather than physiological processes in the human visual system, and the model could only be reliably described for the conditions where visual performance is measurable and quantifiable. Although it may not be possible to confirm visual performance at the extreme ends of the mesopic range, it is unlikely that the discontinuity in the mesopic luminance has a physiological basis.

In cases where use of the iterative model is undesirable or not possible to implement, an approximative formula can be used. We present a set of formulas in equations (9) and (11) for S/P-ratio values $R_{sp} \leq 1$ and $R_{sp} > 1$, respectively. The difference to the iterative model caused by the approximation is smaller than 0.005 for the value of m in most of the mesopic range. This difference causes at most a 0.5% difference in the value of mesopic luminance. At low luminance levels, the deviation of equation (9) increases rapidly due to the discontinuity of the iterative model. The parameterised model approaches the CIE 191 model with increasing luminance and S/P-ratio. To achieve a smooth transition between scotopic and mesopic ranges, it was necessary to relax the requirement of CIE 191 concerning the smallest allowed L_{mes} values. In the CIE recommendation, the adaptation level m is always zero when $L_{mes} \leq 0.005\,cd{\cdot}m^{-2}$. The justification for a definite lower limit is practical implementation, as it would be advantageous to have a clearly defined boundary outside of which no changes are required to a current photometry system. In our parameterised model, L_{mes} can have values below $0.005\,cd{\cdot}m^{-2}$ with positive adaptation levels m, when the S/P-ratio is smaller than 1. The lower limit is then defined such that the vision is purely scotopic only when both L_p and L_s are below $0.005\,cd{\cdot}m^{-2}$.

The benefits of the parameterised model include both providing a smooth function and the possibility of a more robust calculation of uncertainty propagation through partial derivatives. It is also reasonable to assume that a smooth transition between scotopic and mesopic ranges has a better correlation with the human visual system.

Funding

Financial support was provided by the Aalto Energy Efficiency Research Programme (project Light Energy – Efficient and Safe Traffic Environments).

Acknowledgements

The authors thank Liisa Halonen for valuable comments.

References

1 Commission Internationale de l'Éclairage. *The Basis of Physical Photometry*. CIE Technical Report 18.2. Vienna: CIE, 1983.
2 Shpak M, Kärhä P, Porrovecchio G, Smid M, Ikonen E. Luminance meter for photopic and scotopic measurements in the mesopic range. *Measurement Science and Technology* 2014; 25: 095001.
3 Commission Internationale de l'Éclairage. *Recommended System for Mesopic Photometry Based on Visual performance*. CIE Technical Report 191. Vienna: CIE, 2010.
4 Rea MS, Bullough JD, Freyssinier-Nova JP, Bierman A. A proposed unified system of photometry. *Lighting Research and Technology* 2004; 36: 85–111.
5 Goodman T, Forbes A, Walkey H, Eloholma M, Halonen L, Alferdinck J, Freiding A, Bodrogi P, Várady G, Szalmas A. Mesopic visual efficiency IV: a model with relevance to night-time driving and other applications. *Lighting Research and Technology* 2007; 39: 365–392.
6 Sagawa K. Toward a CIE supplementary system of photometry: brightness at any level including mesopic vision. *Ophthalmic and Physiological Optics* 2006; 26: 240–245.
7 Berman SM. Energy efficiency consequences of scotopic sensitivity. *Journal of the Illuminating Engineering Society* 1992; 21: 3–14.
8 Zwinkels JC, Ikonen E, Fox NP, Ulm G, Rastello ML. Photometry, radiometry and 'the candela': evolution in the classical and quantum world. *Metrologia* 2010; 47: R15–R32.
9 Bureau International des Poids et Mesures. *Principles Governing Photometry Monographie 83/1*. Paris: BIPM, 1983.

Appendix: Derivation of the mesopic luminance equation

Photopic and scotopic luminances are given as[1]

$$L_{\mathrm{p}} = K_{\mathrm{m}} \int V(\lambda) L_{\mathrm{e}}(\lambda) \mathrm{d}\lambda \qquad \text{(A1)}$$

$$L_{\mathrm{s}} = K'_m \int V'(\lambda) L_{\mathrm{e}}(\lambda) \mathrm{d}\lambda \qquad \text{(A2)}$$

where K_{m} and K'_m are the maximum luminous efficacy values for the photopic and the scotopic vision, respectively.

Mesopic luminous efficiency and mesopic luminance are

$$V_{\mathrm{mes}}(\lambda) = \frac{1}{M(m)} [m V(\lambda) + (1-m) V'(\lambda)] \qquad \text{(A3)}$$

$$L_{\mathrm{mes}} = \frac{K_{\mathrm{cd}}}{V_{\mathrm{mes}}(\lambda_0)} \int V_{\mathrm{mes}}(\lambda) L_{\mathrm{e}}(\lambda) \mathrm{d}\lambda \qquad \text{(A4)}$$

as given in equations (1) and (2) in the main text.

With equations (12) to (15), mesopic luminance can be expressed as

$$\begin{aligned} L_{\mathrm{mes}} &= \frac{K_{\mathrm{cd}}}{mV(\lambda_0)+(1-m)V'(\lambda_0)} \\ &\quad \cdot \int L_e(\lambda)\cdot[mV(\lambda)+(1-m)V'(\lambda)]\mathrm{d}\lambda \\ &= K_{\mathrm{cd}}\frac{m\int V(\lambda)L_e(\lambda)\mathrm{d}\lambda+(1-m)\int V'(\lambda)L_e(\lambda)\mathrm{d}\lambda}{mV(\lambda_0)+(1-m)V'(\lambda_0)} \end{aligned}$$

$$\begin{aligned} &= \frac{mL_{\mathrm{p}}\frac{K_{\mathrm{cd}}}{K_{\mathrm{m}}}+(1-m)L_{\mathrm{s}}\frac{K_{\mathrm{cd}}}{K'_{\mathrm{m}}}}{mV(\lambda_0)+(1-m)V'(\lambda_0)} \\ &= \frac{mL_{\mathrm{p}}V(\lambda_0)+(1-m)L_{\mathrm{s}}V'(\lambda_0)}{mV(\lambda_0)+(1-m)V'(\lambda_0)} \end{aligned} \tag{A5}$$

This results in equation (3) of the main text when $V(\lambda_0)\approx 0.999998$ is approximated by 1.

Aalto-DD 167/2016
VTT SCIENCE 134

ISBN 978-952-60-6977-7 (printed)
ISBN 978-952-60-6978-4 (pdf)
ISSN-L 1799-4934
ISSN 1799-4934 (printed)
ISSN 1799-4942 (pdf)

978-951-38-8452-9 (printed)
978-951-38-8453-6 (pdf)
2242-119X
2242-119X (printed)
2242-1203 (pdf)

Aalto University
School of Electrical Engineering
Department of Signal Processing and Acoustics
www.aalto.fi

BUSINESS + ECONOMY

ART + DESIGN + ARCHITECTURE

SCIENCE + TECHNOLOGY

CROSSOVER

DOCTORAL DISSERTATIONS